

Mechanical Engineering and Green Manufacturing II

Part 1

Edited by
Shaobo Zhong and Xilong Qu

Mechanical Engineering and Green Manufacturing II

Edited by
Shaobo Zhong
Xilong Qu

Mechanical Engineering and Green Manufacturing II

Selected, peer reviewed papers from the
2nd International Conference on
Mechanical Engineering and Green Manufacturing
(MEGM 2012),
March 16-18, 2012, Chongqing, China

Edited by

Shaobo Zhong and Xilong Qu



Copyright © 2012 Trans Tech Publications Ltd, Switzerland

All rights reserved. No part of the contents of this publication may be reproduced or transmitted in any form or by any means without the written permission of the publisher.

Trans Tech Publications Ltd
Kreuzstrasse 10
CH-8635 Durnten-Zurich
Switzerland
<http://www.ttp.net>

Volumes 155-156 of
Applied Mechanics and Materials *2-vol.-set*
ISSN 1662-7490

Full text available online at <http://www.scientific.net>

Distributed worldwide by

Trans Tech Publications Ltd
Kreuzstrasse 10
CH-8635 Durnten-Zurich
Switzerland

Fax: +41 (44) 922 10 33
e-mail: sales@ttp.net

and in the Americas by

Trans Tech Publications Inc.
PO Box 699, May Street
Enfield, NH 03748
USA

Phone: +1 (603) 632-7377
Fax: +1 (603) 632-5611
e-mail: sales-usa@ttp.net

PREFACE

Dear Distinguished Delegates and Guests,

2nd International Conference on Mechanical Engineering and Green Manufacturing 2012 (MEGM 2012) was held in Hunan Institution of Engineering in Chongqing, China, from March 16-18 , 2012, serving as a platform for expertise exchange. MEGM 2012 had drawn the attention of researchers from various disciplines: Mechanical Engineering Design, Green Manufacturing Technology, Applied Mechanics, Sustainable Materials, etc.

Persons who attended the conference were engineers, scientists, managers of various companies and professors of the universities abroad and home. We have had record number of submission 967 this year. From which 244 papers have been accepted for presentation at the conference and will be published by TTP, in Applied Mechanics and Materials (AMM) Journal (ISSN: 1660-9336), which is online available in full text via the platform www.scientific.net. AMM should be indexed by EI according the previous TTP index results.

We express our special gratitude to all the members of the General Committee Chairs, Program Committee Chairs, Technical Program Committee and Steering Committee who worked so hard to prepare the conference and who supported the conference so professionally.

Our deep thanks also go to the sponsors: National Natural Science Foundation of China, Chongqing University, Hunan Institute of Engineering, Chongqing Normal University, Shanghai Jiao Tong University, National University of Defense Technology, and Xiangtan University, for their kind support in making MEGM 2012 possible.

Finally, we would like to thanks all the authors, speakers and participants of this conference for taking part in and contributing to the International Conference on Mechanical Engineering and Green Manufacturing 2012.

We hope you have a unique, rewarding and enjoyable week at MEGM 2012 in Chongqing.

With our warmest regards,

MEGM2012 Organizing Committees
January 16, 2012
Chongqing, China

Committees

Conference Chairs

Shaojun Liu, Central South University (CSU), China

Dejie Yu, Hunan University, China

Yingchun Liu, Hunan Institute of Engineering, China

Yuanqiang Tan, Xiangtan University, China

Xuejun Li, Hunan University of Science and Technology, China

Hongguang Li, Shanghai Jiao Tong University, China

Program Committee Chairs

Wenjun Xiao, South China University of Technology, China

Yiping Luo, Hunan Institute of Engineering, China

Kexiang Wei, Hunan Institute of Engineering, China

Xilong Qu, Hunan Institute of Engineering, China

Organizing Chair

Shengyi Li, National University of Defense Technology, China

Guobiao Wang, National Natural Science Foundation of China, China

Contact Co-Chairs

Wenjiang Du, Chongqing Normal University, China

Qingmei Xiao, Chongqing University, China

Xilong Qu, Hunan Institute of Engineering, China

Publication Chair

Shaobo Zhong, Chongqing Normal University, China

Technical Program Committee

Yuan Lin, Norwegian University of Science and Technology, Norwegian

Yajun Li, Shanghai Jiao Tong University, China

Mingyi Gao, National Institute of AIST, Japan

Haibing Yin, Peking University, China

Jianxin Chen, University of Vigo, Spain

Miche Rossi, University of Padova, Italy

Ven Prasad, Delft University of Technology, Netherlands

Mina Gui, Texas State University, USA

Nils Asc, University of Bonn, Germany

Ragip Kur, Nokia Research, USA

On Altintas, Toyota InfoTechnology Center, Japan

Suresh Subra, George Washington University, USA

Haiyong Bao, NTT Co., Ltd., Japan

Liang Zhou, ENSTA-ParisTech, France
Hui Wang, University of Evry in France, France
Haining Wang, College of William and Marry, USA
Dumisa Wellington Ngwenya, Illinois State University, USA
Zhao-Hui Jiang, Hiroshima Institute of Technology, Japan
Michael Watts, Lincoln University, New Zealand
Tai-hon Kim, Defense Security Command, Korea
Seong Kong, The University of Tennessee USA
Worap Kreesuradej, King Mongkut's Institute of Technology Ladkrabang, Thailand
Uwe Kuger, Queen's University of Belfast, UK
Tashi Kuremoto, Yamaguchi University, Japan
Chun Lee, Howon University, Korea
Cent Leung, Victoria University of Technology, Australia
Jams Li, University of Birmingham, UK
Liang Li, University of Sheffield, UK
Xiao Li, CINVESTAV-IPN, Mexico
Stefa Lindstaedt, Division Manager Knowledge Management, Austria
Paolo Li, Polytechnic of Bari, Italy
Zheng Liu, Nagasaki Institute of Applied Science, Japan
Michiharu Kurume, National College of Technology, Japan
Sean McLoe, National University of Ireland, Ireland
R. McMenemy, Queen's University Belfast, UK
Xiang Mei, The University of Leeds, UK
Cheol Moon, Gwangju University, Korea
Veli Mumcu, Technical University of Yildiz, Turkey
Nin Pang, Auckland University of Technology, New Zealand
Jian-Xin Peng, Queen's University of Belfast, UK
Lui Piroddi, Technical University of Milan, Italy
Girij Prasad, University of Ulster, UK
Hai Qi, University of Tennessee, USA
Wi Richert, University of Paderborn, Germany
Meh shafiei, Dalhousie University, Canada
Sa Sharma, University of Plymouth, UK
Yongning Tang, Illinois State University, USA
Jun Cai, University of Manitoba, Canada
Sunil Maharaj Sentech, University of Pretoria, South Africa
Mei Yu, Simula Research Laboratory, Norway
Lisong Xu, University of Nebraska-Lincoln, USA
Yan Zhang, Simula Research Laboratory and University of Oslo, Norway
Qishi Wu, University of Memphis, USA

Jalel Ben-Othman, University of Versailles, France
Anru Wu, Hunan Institute of Engineering, China
Dachang Zhu, Jiangxi University of Science and Technology, China
Gaofeng Zhang, Xiangtan University, China
Hongguang Li, Shanghai Jiao Tong University, China
Jiafu Wan, South China University of Technology
Jing Li, Hunan Institute of Engineering, China
Jun Hu, Hunan University, China
Jun Tang, Hunan Urban Construction College
Junan Liu, Hunan Institute of Engineering, China
Kang Ding, South China University of Technology, China
Lianming Zhang, Hunan Normal University, China
Qi Xie, Hunan Institute of Engineering, China
Shanghong He, Changsha University of Science & Technology, China
Wenming Zhang, Shanghai Jiao Tong University, China
Xianghua Miao, Kunming University of Science and Technology, China
Xingzu Ming, Hunan University of Technology, China
Yanchun Zhang, University of Victoria, Australia
Yimin Shao, Chongqing University, China
Yiming Chen, Yanshan University, China
Yongwei Zeng, Hunan Institute of Engineering, China
Yu Luo, University of Electronic Science and Technology of China

Reviewers

Yuan Lin, Norwegian University of Science and Technology, Norwegian

Yajun Li, Shanghai Jiao Tong University, China

Mingyi Gao, National Institute of AIST, Japan

Haibing Yin, Peking University, China

Jianxin Chen, University of Vigo, Spain

Miche Rossi, University of Padova, Italy

Ven Prasad, Delft University of Technology, Netherlands

Mina Gui, Texas State University, USA

Nils Asc, University of Bonn, Germany

Ragip Kur, Nokia Research, USA

On Altintas, Toyota InfoTechnology Center, Japan

Suresh Subra, George Washington University, USA

Haiyong Bao, NTT Co., Ltd., Japan

Liang Zhou, ENSTA-ParisTech, France

Hui Wang, University of Evry in France, France

Haining Wang, College of William and Marry, USA

Dumisa Wellington Ngwenya, Illinois State University, USA

Zhao-Hui Jiang, Hiroshima Institute of Technology, Japan

Michael Watts, Lincoln University, New Zealand

Tai-hon Kim, Defense Security Command, Korea

Seong Kong, The University of Tennessee USA

Worap Kreesuradej, King Mongkut's Institute of Technology Ladkrabang, Thailand

Uwe Kuger, Queen's University of Belfast, UK

Tashi Kuremoto, Yamaguchi University, Japan

Chun Lee, Howon University, Korea

Cent Leung, Victoria University of Technology, Australia

Jams Li, University of Birmingham, UK

Liang Li, University of Sheffield, UK

Xiao Li, CINVESTAV-IPN, Mexico

Stefa Lindstaedt, Division Manager Knowledge Management, Austria

Paolo Li, Polytechnic of Bari, Italy

Zheng Liu, Nagasaki Institute of Applied Science, Japan

Michiharu Kurume, National College of Technology, Japan

Sean McLoe, National University of Ireland, Ireland

R. McMenemy, Queen's University Belfast, UK

Xiang Mei, The University of Leeds, UK

Cheol Moon, Gwangju University, Korea

Veli Mumcu, Technical University of Yildiz, Turkey

Nin Pang, Auckland University of Technology, New Zealand

Jian-Xin Peng, Queen's University of Belfast, UK

Lui Piroddi, Technical University of Milan, Italy

Girij Prasad, University of Ulster, UK

Hai Qi, University of Tennessee, USA

Wi Richert, University of Paderborn, Germany

Meh shafiei, Dalhousie University, Canada

Sa Sharma, University of Plymouth, UK

Yongning Tang, Illinois State University, USA

Jun Cai, University of Manitoba, Canada

Sunil Maharaj Sentech, University of Pretoria, South Africa

Mei Yu, Simula Research Laboratory, Norway

Lisong Xu, University of Nebraska-Lincoln, USA

Yan Zhang, Simula Research Laboratory and University of Oslo, Norway

Qishi Wu, University of Memphis, USA

Jalel Ben-Othman, University of Versailles, France

Anru Wu, Hunan Institute of Engineering, China

Dachang Zhu, Jiangxi University of Science and Technology, China

Gaofeng Zhang, Xiangtan University, China
Hongguang Li, Shanghai Jiao Tong University, China
Jiafu Wan, South China University of Technology
Jing Li, Hunan Institute of Engineering, China
Jun Hu, Hunan University, China
Jun Tang, Hunan Urban Construction College
Junan Liu, Hunan Institute of Engineering, China
Kang Ding, South China University of Technology, China
Lianming Zhang, Hunan Normal University, China
Qi Xie, Hunan Institute of Engineering, China
Shanghong He, Changsha University of Science & Technology, China
Wenming Zhang, Shanghai Jiao Tong University, China
Xianghua Miao, Kunming University of Science and Technology, China
Xingzu Ming, Hunan University of Technology, China
Yanchun Zhang, University of Victoria, Australia
Yimin Shao, Chongqing University, China
Yiming Chen, Yanshan University, China
Yongwei Zeng, Hunan Institute of Engineering, China
Yu Luo, University of Electronic Science and Technology of China

Table of Contents

Preface, Committees and Reviewers

Chapter 1: Green Manufacturing Technology

Application Effects Influenced by Credibility of Simulator Models M. Ding, S.M. Jiao, K.F. Wang and P. Han	3
Improved Ant Colony Algorithm Base on Slab Cluster for Roll Planning H.L. Liang, J. Zhang and B. Hu	7
Study on Performance Optimization of Car Diesel Engine with VNT Based on One-Dimensional Simulation and Experimental Verification L.X. Wang, D.W. Qu, C.Q. Song and Y. Tian	12
A Simple Linear Discrimination Algorithm for AD Patients and Normal Controls Y.Y. Yan, G.Z. Hu, B.L. Guo and Y.J. He	18
Dynamic Analysis of an SIRS Model with Nonlinear Incidence Rate J.H. Li, N. Cui, L. Cui and C.J. Li	23
The Design and Development of a Mass Balance Calculation Software for Sodium-Calcium Dual-Alkali Scrubbing Flue Gas Desulfurization W.H. Pan, Y.X. Shi and J.P. Liu	27
Numerical Simulation of 2-D Two-Phase Flow Field Covered by Vegetation Dam Based on Fluent Software F. Liu, L. Ma, L.L. Chen and G.H. Wei	32
Efficient Data-Parallel Algorithm for Elevation Color Generation in Terrain Rendering Z.K. Zhou, J. Wang and H.C. Zhao	37
Experimental Evaluation on the Effect of the Position of the Nozzle in End Milling under Minimum Quantity Lubrication Condition S.M. Yuan, S. Liu, L.T. Yan and Q.C. Xiong	42
Dynamic Reliability Based on Perturbation Stochastic Finite Element W.H. Mo	47
A User-Engineering Design Interaction Supporting Rational Product Cooperative Design J.J. Qin, Y.A. Yao and J.W. Yang	51
High Precision Reverse Engineering Design for Complex Structural Component Based on Meta Feature W.W. Wu, J. Hong, B.T. Li and Z.H. Yang	56
Research of Case-Based Reasoning System on the Automotive Body Panel Process Z. Wang	62
Application of ARMA Model in Forecasting Aluminum Price Y. Ru and H.J. Ren	66
Investigation into Method of Electric Hot Drilling to Minipore L.Y. Xu, Q. Wu, Y. Mao and Y.Z. Li	72
Study and Realize of High-Speed Data Transmission System Based on MODEM J. Zhang and W. Dong	77
Graphene Oxide Modified DNA Electrochemical Biosensors M. Ma, X.P. Fan, Z. Dai, X. Liu, S.C. Xu, J. Wei, S. Shi and G.P. Chen	82
Rolling Bearing Fault Diagnosis Research Z.H. Yuan, Y. Su and X.X. Qi	87
Improved Shuffled Frog-Leaping Algorithm and its Application J.M. Zhang and C.C. Wu	92
Effective Ways to Realize Green Machining T.F. Li, B.Q. Shi and X.J. Fu	97
Application of Urban Water Demand Prediction Model by Using Particle Swarm Algorithm Based on Simulated Annealing B. Sun, J.C. Xie and N. Wang	102

A Systematic Way of Choosing the Components of HEV and Optimization of Power Management Strategy for Real City Driving Condition C. Chen and J. Li	107
Design of the Remote Environment Monitoring System Based on Virtual Instrument R.C. Sun and X. Son	111
3C Product Design by Customers Based on Geek Net Groups P.H. Li and Z.J. Fan	115
A Novel Numerical Control Architecture Based on Multiprocessor and Real-Time Ethernet W.J. Bu	120

Chapter 2: Mechatronics

Tracking Time-Varying Powerline Interference in Electrocardiogram Using Robust Extended Kalman Filter G.J. Li, S.T. Zhang, N. Xiao and X.N. Zhou	127
Analysis of Contact Stress on Coating Based upon Hertz Theory L.P. Wang, H.D. Luo and Y.M. Cui	133
Node Behavior Trust Evaluation Model Based on Sliding Window Q. Zhu	138
The Application Research in the Evaluation of Sports Teaching Quality Based on the Analytic Hierarchy Process X.F. Wang and X.Q. Wang	143
Adaptive Management of Process Communication Mechanism Base on White Matter Model H. Fang	148
A Request Distribution Strategy Based on Static Time Interval X.L. Xie, Y.L. Zhao and M. Pan	153
The Development and Research of the Three-Dimensional Simulation System of the Garments CAD L.N. Yang	157
Design and Simulation of Direct Drive Volume Control Actuator Y. Yu and B.Q. Shi	162
A SiGe HBT Variable Gain Amplifier for Wireless Receiver System with On-Chip Filter W.J. Zhang and B. Wang	167
A Quick Edit Method of Curve Network's Interpolated Surface Based on Combined Subdivision G. He, D.L. Zhu, M. Zhang and Z.Y. Pan	171
FE Calculation and Analysis of Plain Dent Size Influence on Pipeline Displacement W. Ying, Z. Peng and L. Wu	176
Research on Technical Measure for Rail Potential Reduction D.L. Zhang	181
Based on Genetic Algorithm Research of Stocker Picking Shortest Path F.C. Wan, D. Chen and Y.Q. Wu	186
A Modifying Sub-Threshold Weak Conjugate Gradient Pursuit Method Z.Y. Yang, J.P. Li and E.M. Dong	191
Coupling Evaluation of Concrete Quality Based on PCA-WNN C.H. Huang, Z.R. Lin, G. Bao and Y.S. Lu	196
Analysis the Displacement Amplification of Compliant Parallel Four-Bar Using Piezo Actuator X.F. Yang, W. Li and Y.Q. Wang	201
Optimization Theory in the Application on the Flexible Management of Human Resource X.Y. Jia and W. Wang	206
Chaotic Artificial Bee Colony Constrained Optimization Algorithm with Hybrid Discrete Variables and its Application to Mechanical Optimization Y.X. Luo and X.Y. Che	211
Conversions of Magnetic Anomaly and 3-D Inversion at Low Magnetic Latitudes J.H. Li and Z. Xi	216
Dynamic Trust Model of Internet-Ware Based on Task Classification G.S. Yin and S.Y. Wang	221

Design and Implementation of Surveying Instrument and Equipment Management System Based on VFP	
S. Gou, L.J. Fan and L.T. Xiang	226
A Cognitive Access Selection Approach for Heterogeneous Wireless Networks Based on Fuzzy Logic	
Z.D. Wang, H.Q. Wang, G.S. Feng, X.M. Chen and Q. Zhu	231
Study on CFD Solution Method for Static Characteristics of Hybrid Oil Film Bearing	
D.Y. Li	236
Analysis of the Impact of Government Characteristics on Emergency Management Information System Application	
Y.M. Chen and Y.M. Lin	241
Energy Balancing Multipath Routing Protocol in Wireless Multimedia Sensor Networks	
E.Y. Sun, X.J. Shen and H.P. Chen	245
Research on Information Extraction in Pipe-Routing Layout Space for Complex Products	
X.L. Bai and Y. Zhang	250
Design and Application of New Mushroom Type Center Machine	
R. Li	255
Research on Material Database for Nationwide Fitness	
X. Zhang	260
Research on the Method of MAP Evaluating Based on BP Network	
Y. Yuan and L. Gao	265

Chapter 3: Mechanical Power Engineering

A Theoretical Study for Temperature Condition of Motorized Spindle System	
M. Yang, D. Wang, P.X. Qu and X.J. Li	273
Optimization of the Energy-Saving of the Urban Rail Vehicle's Running	
Y. Hou, J. Yang and Q. Zhang	278
Calibration of Hydraulic Model in Rea-Life Water Distribution System	
W.W. Zhang, G.P. Yu and M.S. Bai	285
<i>Ab Initio</i> Study of the Phonon Frequency, Electrical and Thermal Properties of TiN	
X. Tan, Y.Q. Li and X.J. Liu	291
Design of High-Accuracy Digital Controlled Direct Current Power Supply	
Z.M. Chen	298
Stable and Efficient High-Tension Communication Power Supply Based on Electromagnetic Coupling	
L.M. Li, Y. Chen and Y.B. Wei	303
Research on Temperature Test System Based on LabVIEW	
B. Guo and D.Q. Ren	308
The Application of Electric Current Detection Based on Instantaneous Reactive Power Theory	
Q.Y. Liang, Z. Sun and C.F. Zhang	313
Influence of Surface Texture Configuration and Depth on Tribological Performance of Hydrodynamic Journal Bearing	
S.H. Wang, J.H. Zheng and X.Y. Wu	318
Structure Optimization and Numerical Verification of Plenum Chamber for Relaxation Heat Setting Machine	
S.Q. Song, Y.H. Ge and H.T. Zhao	324
Doubts of Calculation of Efficiency Transmission of CHT-100 Type Circulating Power of the Efficiency Transmission Gear Experiment Set	
Y. Zhao and Q. Yan	331

Chapter 4: Signal Processing and Fault Diagnosis

Research of FRFT Rotation Factor Sensitivity and Diffusion Based on Audio	
J.G. Jin, C. Chen, M.J. Wei and L.C. Xia	337

An Efficient Distance and Density Based Outlier Detection Approach X.B. Zhong and X.X. Huang	342
Wear Reliability Analysis Method Based on Random Process Y.T. Yan, Z.L. Sun, G.W. Hu and L.F. Liu	348
Research of Security Mechanisms Based on LogicSQL Database D.N. Li, Q. Li and X.Q. Ma	352
Survey on Collaborative Awareness Model for CSCW and Trends of the New Age J. Wang and D.W. Chu	357
Robust Optimization Design and Evaluation to Five Roller Coating Module without Solvent Based on Axiomatic Design Q. Cheng, C.M. Xiao, J. Zhang, L.G. Cai and P.H. Gu	363
Virtual Boundary Integral Method for Anisotropic Potential Problems X.R. Jiang and X. Fu	370
Word Similarity Algorithm Based on WordNet And HowNet W.L. Ren and J.J. Guo	375
Particle Simulation of Slow-Wave System in Multi-Beam Traveling Wave Tube Z.L. Li, Y.J. Huang and Z.C. Huang	381
Optimization of the OOP Children Restraint System Z.H. Bai, J. Fei and W.J. Ma	386
The Design of Unified Identity Authentication and Single Point Login System Y.J. Yang	391
On the Mean Value of a New Arithmetical Function M.J. Wang	396
Steel Tube AS/RS Shelf Structure Design and System Layout W.M. Liu, A.Y. Zheng, C.G. Lu and Y. Tang	401
Computations of Hamiltonian Homeomorphisms under Symplectic Reduction in the New Sense D.W. Sun and J.R. Liu	406
An Agent-Based Auto-Negotiation Mechanism with Semantic Web Services W.L. Ren and W. Luo	411
Research on Sports and the Development Humanistic Sports H.Q. Liu	416
Fractal-Based Newton Method and Mechanism Synthesis & Approximate Synthesis Y.X. Luo and L.F. Li	420
Pattern Search for Generalized Hyperbolic Distribution and Financial Risk Measure X.F. Chen and G.B. Chen	424
Android Development and Mobile E-Commerce Research Y.J. Liu and Z.P. Liu	430
Robust Tracking Time-Varying High-Frequency CW Telegraph Signal G.J. Li, X.N. Zhou, N.Q. Liu and S.H. Li	435
Enhanced Three-Dimensional Color Conversion Based on Discrete Wavelet Transform H. Yan and X.F. Wang	440
Three-Dimensional Wireless Sensor Network Localization Algorithm Based on DV-Hop F.C. Wan and Y.J. Shen	445
The Determination of Best Bid Price Quotation Based on Game Theory S.D. Xu, X.L. Cai and W. Liu	450
Speed Torque Measurement System Design of Micro Harmonic Drive S.Y. Chen and H.B. Xin	455
The Research on Scientific Research Management System Based on Improved MVC Pattern C.X. Chen and R. Zhang	459
Intelligent Household Application Base on Mobile Phone Y.X. Zhao	464
Intelligent Household Application Base on Mobile Phone the Ultrasonic Nondestructive Testing Technology Based on the Signal Processing Technique S.P. Wei	470
The Layout of Strain Sensor Based on the Preanalysis Load Distribution Y. Lu, S.L. Zheng, J.Z. Feng and L.H. Zhao	474

Research of Automatic Marking on Access Skill Assessment Based on XML Y.F. Chen	479
---	-----

Chapter 5: Applied Mechanics

Application of the Meshless Local Petrov-Galerkin Method in the Elasto-Plastic Fracture Problem of Moderately Thick Plate P. Xia and K.X. Wei	485
Optimization Research for the Motion Law of Vice-Spindle of Twin-Spindle CNC Turning Center J.H. Liu, H. Jin and H.Y. Niu	491
Wear-Resistance of Die Steel with Non-Smooth Surface Used to Pressure Casting Die Processed by Laser L. Chen, T.J. Li, Z.W. Han and J. Chen	496
Wear of Throwing End of Vertical Shaft Impact Crusher J.M. Zhang	501
Study of Forward Connecting Rod Combined Lifting Mechanism Based on Linear Transformation and Vector Algebra M.Q. Wu	505
The Study of Electromechanical Brake Device Based on the Ball Screw D. Guan, X.H. Yang, G. Liu, R.T. Tong and S.J. Ma	509
Modal Analysis and Design on the Base Plate of Large-Scale Linear Vibration Screen X. Du	514
Study on the Oil Film Static Performance of Sliding Bearings with Different Throttling Methods D.Y. Li and G.Y. Jiang	519
The Design of CNC Lathe Cutting Force Signal On-Line Monitoring J.B. Zhao	526
Analysis of the Multi-Tooth Meshing Effect of Three-Ring Gear Reducer Y. Li and C. Zhu	531
Numerical Simulation on Dynamic Behavior of Intermittent Roller Chain Drives L.X. Xu and Y.G. Li	535
Design of Hydraulic System of Subsea X-Tree H.L. Zhao, J. Yu, Y.L. Yue, S. Li and B.Q. Guo	540
Human Kinematic Characteristics during Stair Descent G. Tang, H.J. Yang, D.F. Chang, D.M. Wang and G.F. Wei	545
Study on Transient Response Analysis and Fatigue Life Evaluation of Water Pump Volute Casing under Impact Load M. Li, Z.H. Yin, K. Shi, J.X. Liu and H.Y. Du	550
The Error Analysis of Gyroscope Drifts to the Rate Azimuth Platform System F.L. Wang, X.L. Wen and D.X. Wang	555
Analysis and Design of a New Digital Interphone H. Li	561
The Precision Analysis on the Force of Connecting Rod in Automobile Engine Based on Unigraphics L.J. Yang	565
Reliability Calculation and Perturbation Stochastic Finite Element W.H. Mo	570
Virtual Design Technology of Piston Production Line Based on Lean Production P.H. Li, J. Zhou and J.X. Deng	574
Effects of Al Content on the Microstructures and Oxidation Resistance of Cr_{1-x}Al_xN Films Synthesized by Multi-Arc Ion Plating Method Z.H. Cai, Y.L. Di, Z. Yang and P. Zhang	579
Research the Influence of Comprehensive Materials Multimedia Technology on the Exercise Interest of Students Q.P. Chen	585
Research on the Guidance Methods of Sports Training Based on Data Mining Technology Q. Zhou	590

Study on Chip Morphology of Electric Hot Minipore Drilling L.Y. Xu, Q. Wu, Y.Z. Li and P.X. Qu	596
Research on Virtual Hobbing Simulation and Study of Tooth Surface Accuracy of Involute Helical Gears X.L. Zhang, Z.H. Wang and G. Li	601
Cusp Catastrophe Intelligence Combinatorial Prediction of Land Subsidence C.H. Huang, Y.S. Lu, G. Bao and Z.R. Lin	606
Process Design of Tacking and Welding for Turbine Blades and Positioning Plates J.H. Song	611
Flow Patterns Transition Criteria from Bubbly to Slug Flow during Flow Boiling in Confined Vertical Narrow Rectangular Channels W. Chang, S.S. Zhang, C. Zhao and Y.L. Zhang	616
The Embedded Audio Coding of Algebraic Quantization Based on the Transform Coefficients G. Tang	621
 Chapter 6: Mechanical Engineering Design	
Discussion of the Modern Electronic Technology Application and Future Development Trend on Automobile J.S. Chen	627
Study on the Integration Technology of After-Treatment System of the Diesel of Heavy-Duty Machinery Y. Tian, D.W. Qu and L.X. Wang	632
The Comparative Research on Air Quality of Natural Ventilation Unit and Air Conditioning Unit in Hospital Building L. Gong, H. Zhou and C.H. Liu	637
Back-EMF Zero-Crossing Rotor Position Detection Control of BLDC Motors X.K. Zhao	643
Modeling and Analysis of Three-Parameter Power Shift Schedule for Pure Electric Bus of AMT L.P. Luo, J.Q. Xi, X.L. Liu and Y.H. Hu	648
The Intelligent Scheduling Method of Elevator Group Control Based on Fuzzy Neural Network Y.L. Dong and X.M. Wang	653
An Online-Monitoring System of Machine Tool Cutting Force C.Z. Wu	658
Integration and Implementation of Numerical Design and Manufacturing Data Management System for Beverage Bottle C. Lv and X.H. Pan	663
Study on High-Frequency Quenching of Steel Tube Screw Thread Lined Glass Used for Petroleum Pipe Line L. Chen and X.M. Liu	668
Discussion on the Optimization Design of Feature Extraction Methods of the EMG Signal Z. Lou	674
Existence of Nontrivial Positive Solutions to a Semilinear Elliptic System with Variable Coefficients D.W. Sun and J.R. Liu	678
Exploration on Infiltrating Human Education in the Basic Chemistry Courses of Science and Engineering L. Han	682
Design and Analysis of Rubber Core with PTFE Ring in Ram BOP Y.K. Fu, C.J. Han, J. Wang and Y. Yi	686
Modeling and Validation of Moving Deformable Barrier Model with Taper Section Beam Element L.B. Cao, W.T. Cheng, R.F. Zhang and J.H. Shao	691
Divisibility Forecast of Air Cushion Vehicle's Motion in Wave N. Ji	696

Exploration and Discuss for Calculation of Efficiency Transmission of JG150 Type Gear Trial Set Y. Zhao and Z.H. Huang	701
Internet-Enabled Calibration Using Virtual Instrument Instead of Traveling Standard J. Wang, Q. Zhang, S.L. Wu and Z.H. Wang	707
The Forming Method of Cylindrical Parts with Bars X.P. Bai	712
Cultivate High Quality Creative Mining Engineering Talents Based on the Construction of Professional Characteristics Z.Q. Kang, Y. Wang and F. Nan	717
Design of Sand Washing and Plug Removal Device with High Pressure Foam Fluid Jet W.B. Cai, G.W. Qin and Y. He	722
Design of the Conjugate Cam Induction Hardening Mechanism and Establishment of the Motion Controlling Mathematical Model Z.H. Li, Q. Tang, D. Yan and J. Wu	726
Study for Traditional Spinning Wheels and Looms in ZE Zhou Region W. Lu and X.M. Yang	731
Separating Nonstationary Powerline Interference from ECG Using Empirical Mode Decomposition G.J. Li, X.J. Hao, H. Zhong and X.N. Zhou	736
Analysis on Laser Welding of Hard Alloy Circular Saw Blades Q. Wu, L.Y. Xu, X.B. Yuan and Y.Z. Li	741
The Research of the Wheel Loader Working Device W.W. Zhang, J. Zhou and J.X. Deng	746
Design and Research of Testing Soil for Forest Formulated Fertilization System L. Yao and N.H. Wang	751
Advanced Method for Mechanical Reliability Design X.J. Fu, B.Q. Shi and T.F. Li	756
Research on 3D Parametric Modeling and Virtual Assembly of Involute Modification Spur Gear Based on Solidworks Z.G. Li	761
Study on Data Acquisition for Heavy Off-Road Vehicle AT Testing E.L. Wang, H.Y. Chen, G. Tao and Y.H. Hu	765
Application of ACO-SVM in Chinese Text Feature Selection J.X. Cui and X.X. Huang	770

Chapter 7: Optical and Electronic Materials

Study on Axial Contact Deformation of Planetary Roller Screw X.C. Zhang, G. Liu, S.J. Ma, R.T. Tong and H. Luo	779
Application of Multi-Beam Technique in Microwave Tubes Z.L. Li, Z.C. Huang and Y.J. Huang	784
Research on Nondestructive Image Compression Technology Based on Genetic Algorithm J. He and H. Guo	789
Study of Residue Stress and Phase Structure of c-BN Films with BNx Implanted Buffer Interlayer on High Speed Steel Substrate J.W. He, Z.H. Cai, Y.L. Di and Z. Yang	795
Reconstruction of the Stone Tablet Based on Vectorization of Images J. Zhang	800
The Application of Heuristic Method in Images Pseudo Coloring W.D. Liu, X.Q. Zhao and W. Zheng	805
Research on 10.6μm Laser Disturbance to Infrared Detector System Y.W. Liu	810
Dual Video Watermarking Scheme Based on Transform Domain Z.W. Gao, Y.M. Zhang, C. Liu, J. Geng and D.K. Ba	815
Application of Multi-Mode Combined Polishing to Optical Manufacturing X.H. Wu	820

Implementation of the Real-Time Parameters Monitoring System for Underground Equipments Based on Panoramic Images B.Q. Shi, C.G. Zhao, Z.J. Hao, M.C. Xu and C.T. Bian	825
Simulation Analysis of the Anti-Settlement Dehydration of the Phosphate Ester Fire-Resistant Oil Based on Lab VIEW X.M. Zhang, J. Yuan, B. Chen and H.W. Lu	831
Research and Application in Image Processing Technology Based on the Embedded Parallel Computing G.M. He and M. Wang	836
Hail Identification Analysis from Radar Image by CNN G.D. Li, X. Wang, F. Zhao and W.X. Xu	841
Simulation of the Cracking Behavior for Fiber Reinforced Composite Materials with the Infuence of Depth-Width Ratio and Direction Angle J.X. Luo	846
Image Refinement in the Application of Fingerprint Identification B. Feng, L.J. Zhang and H.T. Zhang	851
The Control of Humidification and Dew Condensation by Using of On/Off Control of the Bubble Humidifier in the PEMFC Y.G. Jung, H.S. Choi, D.H. Kim and D.H. Park	856
PCNN Based Welding Seam Image Segmentation Algorithm B.J. Zou, H.Y. Zhou, Z.L. Chen, H. Chen and G.J. Xin	861
An Adaptive Image Fusion Method Based on NSCT and AGA J.F. Li and W.Z. Dai	867
Relationship of Post Treatment Temperature and Tensile Strength for Selective Laser Sintering J. Su, X.J. Li and P.X. Qu	872
Effect of CeO₂ on Microstructure and Hardness of Roller Surface Alloyed by Laser H.J. Yue and Q.B. Liu	877

Chapter 8: Sustainable Materials

Studies on Nanoscale Sliding Contacts of Textured Surfaces by Multiscale Method R.T. Tong, G. Liu and L. Liu	883
Case Study of Optimal Material Suppliers Selection by the Value Engineering Theory Y. Liu and Q. Wei	887
Influence of Multimedia Communication Materials on the Students' Sports Motivation M.C. Liu	892
Empirical Research on Comprehensive Materials Multimedia English Classroom Y.Q. Wang	897
Application of Composite Materials on Sports Equipments J.L. Wang	903
Preparation of Layered Double Hydroxides Nanomaterials via the Anionic Surfactant L.N. Sun and W.W. Tang	907
The Exploration on Strategy and Practice of Developing Low-Carbon Tourism A.J. Hu	912
The Effect of Roxarsone on Soil Enzyme Activities J.X. Sun, L.Z. Guan, Y. Zhang and G.C. Zhang	917
Influence of QPQ Treatment on the Corrosion Behavior for Carbon Steel F. Sun, W. Cai, F.N. Meng and J. Hu	922
Mechanical Properties of Ti_{1-x-y}Al_xSi_yN Nanocomposite Studied by <i>Ab Initio</i> X. Tan, Z.Y. Xin, X.J. Liu and Y.Q. Li	926
Study of Erosion on Metal Materials for High Pressure Pipe Manifolds J.X. Zhang, J.C. Fan, X.J. Zhan and X. Jiang	931
Study on O² Plasma Surface Modification of Aramid Fiber III J.Y. Ji, Z.X. Huang, Q. Su and Z. Chen	936
LURR as a Grid Service F. Liang, H.M. Guo, S.W. Yi and S.L. Ma	940

A Study on the Relationship Between China's Energy Consumption and Economic Growth J. Li and Z.T. Zheng	945
Influence of Comprehensive Materials Multimedia on the Students' Sports Motivation X.H. Zhou	950
Effect of Different Grinding Time on the Performance of Gypsum Mould C. Chen, X.Y. Gu, Y.X. Chen and T. Luo	955
ELID Grinding Technology of Nano-Material Cutting Tool J.C. Kuai, F.H. Zhang and Y.Z. Liu	960
Experimental Study of Laser Surface Treatment of Low-Carbon Ductile Iron Y.Z. Li and J.P. Liu	965
Corrosion Behavior of Molybdenum in Molten Aluminum H.F. Luo, J. Wu, Z. Liu and W.P. Chen	969
Influence of Negative Bias Voltage on the Microstructure and Tribological Properties of CrTiAlN Composite Films Z.H. Cai, Y.L. Di, Z. Yang and P. Zhang	974
The Influence of Professional Shoe Materials for Aerobics on Bounce Action of Athletes X.L. Yang	979
Carbonation Depth Research of Concrete with Low-Volume Fly Ash C.H. Huang, G.L. Geng, Y.S. Lu, G. Bao and Z.R. Lin	984
Research on the White Noise Suppression by Adaptive Filtering of Genetic Algorithm X.R. Tong	989
Error Analysis on the Determination of Moisture in Oil by Karl Fischer Method X.M. Zhang, Y.B. Zhang, B. Chen, P. Li, Y.C. Guo and J.H. Li	995
Safety Analysis of Casing with Considering Strength Degradation in Steam-Injection Well H. Tong, X.H. Zhu, S.H. Liu and C.S. Shi	1000
Preparation and Properties of Poly(vinylamine/acrylonitrile) Fiber Q. Chen, R. Xu and D.H. Yao	1005
Design of Parsing Framework with SWF File Y.F. Chen and Y.H. Ni	1009

Chapter 9: Vibration and Control

Precision Water Distribution Control of New Type Sewage Distributor Y.S. Hao, K.S. Ji and Z.Y. Liu	1015
Design of Control System for Welding Tractor Based on DSP Z.H. Yuan, Y.Q. Wu and J.H. Wang	1020
Research on MPLS Network Topology Aggregation Algorithm With The Effective Connected Dominating Sets J. Feng, S.Q. Ma, M.H. Fan and K.N. Wang	1025
Enterprise Green Supply Chain Management in Low-Carbon Economy Model M.Q. Zhu and Y.B. He	1030
The Development of Engine Cylinder Pressure Intelligent Micro Detection System B.H. Zhong	1035
Effects of Ball Screw Empty Rotating on Grinding Error Compensation Performance J.L. Guo, L.Q. Chen, J. Chi and X. Yang	1040
Evaluation and Optimization of Research Projects Based on Grey Relational Analysis Method M. Li, J.J. Wang and J.Y. Wang	1045
Novel Torus-Involute Gear Transmission L. Liu and Z.Q. Huang	1050
Prediction of Ground Settlement Based on Immune Genetic Algorithm G.Q. Bi	1056
Control System Development Based on Arc-Submerging Welder for Flat Fillet Seams G. Wang, L.N. Feng and X.M. Zhang	1061
Vertical Shaft Impact Crusher Wear Analysis and Research on Antiwear Measures Y.Y. Wu	1066

The Analysis on Sports Starting Technology Based on Biomechanical Analysis Method B.H. Ma	1070
On-Line Centralized Path Planning of Multiple Mobile Robots in Dynamic Environments Z.H. Zhang and Y.S. Xiong	1074
Application of NASTRAN Finite Element Analysis and Experimental Test on Loading Machine Structure Strength Analysis Q.S. Tian	1080
FEM Analysis on Block Vibration of Diesel Engine P.P. Guo and W.Z. Gao	1086
Kinematics and Workspace Analyses of 3/3-RRRS Parallel Manipulator M.S. Liu, Y. Cao, Q.J. Zhang, C. Gosselin, J.C. Sun and B.K. Li	1090
Effect of Process Parameters on the Mechanical Properties of Friction Stir Welded Al-Li Alloy Butt Joints D.D. Zhang, W.Q. Qu, Q. Meng, P. Chai, G.H. Luan and J. Chen	1096
Design of the Clutch Friction Plate Temperature Acquisition System Based on Zigbee X.L. Liu, J.Q. Xi, L.P. Luo and Y.H. Hu	1102
Allowable Stress Design of Rupture Strength Based on Confidence Level of 9Cr-1Mo Steel J.B. Pei, Y.F. Zhao, S.P. Yu and J. Zhao	1107
Development on Pill Feeding Vehicle Control System for Packaging Workshop of Traditional Chinese Medicine R. Yan	1112
The Analysis of ATM Queuing Phenomenon on Campus N. Song and Z.Q. Shang	1117
Design Concept Evaluation and Selection: A Decision Making Approach R. Ullah, D.Q. Zhou and P. Zhou	1122
The Coupling Effect between Aerobic Exercise and Physical & Form of the Youth Y. Chen, A.M. Qin and B. Su	1127
Finite Element Analysis on the Brake Shimmy of Drum Brake Y.Q. Xu, Q.W. Zhang and J.H. Zhao	1132
The Application of SIFT Algorithm in Blind Road Environmental Image Matching S. Shi, M. Yu, C.H. Xue and Y. Zhou	1137
Influence of Blade Thickness on Unsteady Propeller Forces M.Z. Chen, Q.D. Zhou and Z.Y. Xie	1142
The Application of Fuzzy Theory in Automatic Checking over Subjective Examination S.Y. Gao	1147
Effects of PCL Deficient on Biomechanics of Knee's Cartilage and Menisci at Different Flexion Angles R.Y. Huang, G.L. Zhang, Y.F. Guo and H.G. Zheng	1153
Braking Performance Study for Automobile with Numerical Simulation X.Y. Zhang, P.X. Qu and X.J. Li	1159
An Improved Algorithm of Underwater Target Feature Abstracting Based on Target Azimuth Tendency Y. Xu, B.C. Yuan and H.G. Zhang	1164
Prediction on Number of Agricultural Pumps in Henan Province of China Based on BP Neural Network J.W. Li, X.S. Wang and Y.G. Tang	1170
Design of Personalized Intelligent Information Retrieval Model Based on Agent Z.B. Sheng, H.P. Jia and X.R. Tong	1175
Temperature Numerical Simulation of Friction Stir Welding Process of Radar Cooling Board L. Wang, J.J. Zhu, K.Y. Yin and H. You	1180
Contrast Test on Fender Forces Between Flexible and Rigid Berthing Systems J.H. Liu, K.L. Shen, H.Y. Ding and J.H. Diao	1184
A Modification of Adaptive Control and Synchronization of a New Hyper-Chaotic System with Unknown Parameters Y.L. Cheng, J.W. Lei and W.G. Zhang	1189
The Time Series Design of Profibus-DP Slave Based on FPGA Z.P. Chen and Z.X. Qiu	1193

The Research on Fuzzy Apportionment of Pump Product Based on FMECA M.W. Hou	1198
Analysis of the Influence of Fillet Curves on Gear Bending Strength Based on Space Contact Z.H. Wang, N. Zhang, D.M. Dong and X.J. Chen	1203
Forward Kinematics Analysis of a Multi-Axis Linkage Wire-Cutting Robot Based on ADAMS Y.C. Jiang, C.L. Zhang, Z.W. Sun, F.W. Xie and Z.F. Zhang	1208
Rod Orifice Hydraulic Absorber and Application for Impact Crash Simulation Q. Li and H.B. Ren	1213
Comparison of Residual Stress Between MIG Welding and Friction Stir Welding L. Wang and M. Tsunori	1218
An Improvement of PISS Integral Sliding Mode Control of Supersonic Missiles G.Q. Liang, J.W. Lei and X.J. Shi	1223
Chatter Stability Modeling and Simulation for Long Slender Shaft Turning Operation S. Li, Z.Q. Li and M. Zheng	1227
Research to the Liquid Level Control of Water Tank Based on Fuzzy Immune PID Controller H.Z. Chen	1232
Research on Multi-Layered Modular Experimental Teaching System of the Public Management Specialties M. Song	1237

CHAPTER 1:
Green Manufacturing Technology

Application Effects Influenced by Credibility of Simulator Models

Man Ding^{1,a}, Songming Jiao^{1,b}, Kunfang Wang^{1,c}, Pu Han^{2,d}

¹ Department of Automation, North China Electric Power University, China

²Hebei Engineering Research Center of Simulation & Optimized Control for Power Generation, North China Electric Power University, China

^adingman1987@126.com, ^bjiaosongming@126.com,

^cwang_kunfang@126.com, ^dhanpu102@263.net

Keywords: Thermal power plant; Simulator; Application; Accuracy; Credibility.

Abstract. This paper introduces how the simulator's credibility, which mainly includes the fidelity and accuracy, influences the practical application effects. Based on analyzing the factors that influence the physical fidelity and the mathematical model accuracy, an approach is put forward to improve the simulation precision. Furthermore, the paper summarized the practical values of the simulator and its function on scientific research.

Introduction

Thermal power unit simulator has already been applied to pre-job training for centralized control personnel, proficient operation training and evaluation of the workers, etc. Because impelled simulation technology based on virtual DCS has come up during past 10 years [1], the application field was enlarged to training and evaluation on thermal control personnel. Nowadays, a number of users are coming up with the ideas that simulator could be applied to the accident reconstruction and analysis, the revision of the operation rules, the test and evaluation of the control system of power plant configuration and so on. In order to implement these functions, we should improve the precision of the simulator firstly. As a matter of fact, the above functions can be realized in the early simulators [2]. However, due to the technical and economic reasons, most of the users do not put forward these requests before.

The credibility of the simulator mainly includes the fidelity and precision. The fidelity of the simulators denotes the level of similarity between simulator and actual power station in the equipments (such as meters, switches, press-buttons, pilot lamps, CRT displayers and keyboards, etc.) and control room environment on appearance, shape, size, color and location. We can call this fidelity as physical fidelity. The higher the level of similarity is, the higher physical fidelity is. There are many factors which only want to get ideal training effect [2]. The precision of the simulator is referring to the simulator precision in the simulation proceeding of static and dynamic response. The precision of the simulator could be called as the physical fidelity or function fidelity. It can be categorized simulator software and mathematical model. The precision of the simulator includes transient and steady precision accuracy. This paper discusses the credibility's influence on the effects of the various applications.

The effects on operators in the power plant caused by physical fidelity

The effects caused by the operator station

Stimulated simulator based on virtual DCS has completely copied all of the functions of the actual DCS and the logic structure of the system is same to the practical process logic. It is easier to be understood, to be used and to be completely imitated from appearances, computers used by operator's station to displayers. Hence, stimulated simulator based on virtual DCS will not reduce the application effect either applied to training or study.

The effects caused by the surroundings in the simulation room

The surroundings in the simulation room refer to the indoor decoration, brightness, sounds (environmental noises), etc. except the operator station. These facilities which are seemingly have nothing to do with the simulator precision will impact greatly on operator training result. This is mainly caused by human psychological factors. If the size of the simulation room, the color of the wall, the shape, power(brightness) and position of lights are same to the simulated power plant's are also same to the simulated power plant's, and then produce same environmental noise through the sound system (these are easily to be realize), all of which could make the trainers feel to be personally on the scene. All of that are especially important factors for beginners, they can identify different accidents though the brightness of the lights. But as for experienced people, they will forget wither they are in the simulation room or at the actual scene, it will significantly improve trainees' attention, so as to enhance the training effect.

The effects caused by the furnace flame monitor

Trainees can watch the position and shape of flame, monitor the combustion status from flame monitor and then analyze wither the combustion is normal or not. At present, we realize this function by use of large capacity images stored laser flay back equipment. The video equipment stores all kinds of combustion information in the laser video disc. It will plays according to different working condition under the control of computer. The monitor's fidelity will be influenced by response speed and switching speed of the flame images. The monitor's fidelity can also influence trainees' operating experience. If we make high flame monitor fidelity, trainees can get combustion optimizing experience. When they use these experiences to the actual operation, it will achieve the objective of saving energy and reducing emission.

Main factors that affect the accuracy of the simulation mathematical model

The main factor that affects the precision of the simulator is the simulation power station of heating equipment mathematical model. In recent years, the development of mathematical model technology is rapid. The description of the mathematical model of local power station process is more and more accurate, but that is not to say the whole mathematical model is accurate. That's because when we set up mathematical models of equipment, we usually do some simplification and neglect. So once each subsystem models are put together, the overall precision of the model will be worse. In order to get enough simulation precision, we must modify local model of simulator constantly during the simulator producing process [3]. Main factors that would affect the accuracy of the mathematical model simulator are as follows:

Effects caused by the mathematical model simplification

All of the boilers, turbines and generators in thermal power plants have complicated structure and huge shape. Generally, we divide them into several typical subsystems and then establish the mathematical model of each subsystem respectively. Finally, we combine them into the whole system's model. In addition, we always regard the distributed parameters that along the three dimensional space as lumped parameters; in other words, we always take time parameter items into account and ignore the space distribution of parameters. For example, boiler furnace temperature is different everywhere, however, we take it equivalent to a particular furnace, and the temperature is the same everywhere. Single-phase media heat exchanger such as super-heater, re-heater and economizer are simplified as the equivalent heat pipe. We regard the metal temperature of the whole pipe are same everywhere; the heat only transfer along radial direction. Because it is very difficult to get a distributed parameter models, we usually use lumped parameter system model of the thermal power station. This is a kind of inevitably hypothesis and that will inevitably affect to the accuracy of the mathematical models.

The impact of coefficient selection on mathematical modeling

From reference [2] we can know that the parameters in formula whose parameters are simplified and lumped are gotten from mass-conservation equation and energy conservation equation calculation. In engineering practice, the model parameters in these formulas are set by way of trial and error, so errors necessarily exist in the system.

Effects of digital simulation algorithm choice on the accuracy of the mathematical model

Digital simulation algorithm includes Euler formula, trapezoidal formula, fourth order Longe-Kutta formula. Reference [2] indicates that Euler formula's computing speed is fast, but the calculation accuracy inferior to the trapezoidal formula and fourth orders Longe-Kutta formula. The popular algorithm in thermal power plant simulator is Euler's formula. By simulation, we find that in the condition of small simulation step (display instrument don't show up the phenomenon of jumping), the accuracy of the Euler's formula is close to the fourth order Longe-Kutta formula's. Furthermore, the calculation speed of fourth order Longe-Kutta formula is slower than Euler's formula. As we all know, calculation speed of the computer itself is fast enough nowadays. We needn't to use fourth order Longe-Kutta formula which only superiority is of high accuracy of calculating. One more reason for not using fourth order Longe-Kutta formula is that errors through 3.1, 3.2 cannot be improved by fourth order Lo Longe-Kutta formula.

The effects of the simulator precision on training and scientific research

With the expansion of the scale of the power plants, the unit plant is developing towards the direction of large capacity, high parameter and high automatization. In order to make sure that the power plant units run safely and economically, the personnel in power plant should be trained and educated constantly, so they can analyze the systems in the power plant, and make researching and designing. In this process, the simulator plays an important role. In different application aspects, it puts different requirements on the simulator's precision.

At present, simulated simulator based on virtual DCS has been widely used. Its simulating environment has been realized to the same to the actual environment. Hence, the simulator precision mainly refers to the simulator's mathematical fidelity. That is the precision of its mathematical model.

The simulator applied to training thermal control personnel

In power plants, we use simulators to train thermal control personnel to master the operation of starting up and stopping the equipments of the units, and train them to master the technical knowledge such as process controlling and functional configuration of the DCS systems of the units. As for this application, we should first make the parameters' changing trend of the simulator are corresponding to the changing trend of the actual power plants. In the process of transient operating, all parameters' trends should not damage the authenticity of the simulation, we don't need to put forward excessive demands on the simulator's precision.

The simulator applied to training centralized control personnel

The centralized control personnel in power plants should make sure that the unit operates safely and economically, when malfunctions occur, they should discern them and deal with them in time. In the power plants, we use simulators not only to train centralized control personnel to master the operation of the units in formal condition, but also train their ability to analyze and solve the problems when different kinds of malfunctions occur. Because centralized control personnel are the monitoring personnel who directly control the operating of the power plants, they should have clear cognition of the operation in every working condition and the changing of every parameter in the power plant, so it sets forth stricter requirements for the simulators in the power plants.

According to the '*Industrial Standard of the Power Plant Simulator*' in our country, when the load is higher than 25%, for example, 50%, 75% and 100% load, the static error of the calculated value of the key parameters should be less than 2% when compared to the designed value of the reference power plant. The error of the calculated value of the non-critical parameters should be less than 10% when compared to the designed value of the

reference power plant. As for the error of the transient state, it calls for a lower requirement, it is because that the mathematical model we set up is hard to make high-precision in the whole dynamic process, the mathematical model only can calculate accurately in certain working conditions. We need the simulator's precision at the transient state to meet the following requirement: when compared to the actual power plant, the error of the key parameters of the simulator's transient response should be less than 10%.

In order to get a more accurate mathematical model, we should modify the parameters of the model using experts' experience or other test methods in the debugging process^[4] until it needs the simulator's requirement.

The simulator applied to scientific research

The simulator of the thermal power plant not only provides a good training platform for the thermal control operators, but also creates a real-time and on-line environment for experts to analyze the operating technology and researching the control system. Experts can use it to conduct research in all kinds of operation ways of the thermal units. They can make computational analysis for the technological and economic indicators of the units based on the information in different working conditions, then optimize the units' operating mode and strategy under effective ways to make the units operate safely, economically and efficiently. In addition, simulators can recur actual power plant's malfunctions. Experts use this useful information to analyze and diagnose the malfunctions, to test and verify the cause and effect of the malfunctions, then find out the countermeasures of eliminating these malfunctions. To realize these functions, we should improve the precision of the simulator models.

In order to make the simulators' precision to meet the need of scientific research, during the simulator being debugged, the parameters of the models should be modified constantly; even the mathematical model should be rebuilt until the simulator's precision meets the requirement. We should use distributed parameter models when a more precision model is needed.

Summary

The power plant simulator can be widely used in variety of fields. For different applications, different demands on the accuracy of the simulators will be needed. If the simulator just used for training power plant students, the simulator should have high fidelity in physical appearance. The students will be familiar with the operation of the power plant process and the surroundings in the short time and master all kinds of actual operations. If the simulator is used for scientific research, we should mainly focus on improving simulator mathematical model of the fidelity to make the operation parameters be close to actual parameters in power plant. So expert could get more effective information from the simulator and then they can use this information to analysis and optimize the thermal power unit.

References

- [1] P. Han, Y. J. Zhai, L. Z. Wang: The Analysis and Design of Simulated Simulators Based on Virtual DCS System[J]. Journal of North China Electric Power University, Vol. 32(2) (2005), p.37-40.
- [2] P. Han, C. L. Liu, C. Q. Li: The Theory and Application of Thermal Power Station[M]. Tian Jin: Tianjin Science and Technology Publishing House (1998).
- [3] F. Q. Liu, G. Q. Zhao: Debugging on simulator Mathematical Model of Thermal Power Station[J]. Ningxia Electric Power Vol. 2 (2004), p. 4-10
- [4] M. Sun, M. Ding, S. M. Jiao, K. F. Wang, P. Han: The Research of Validation Methods for large Thermal Power Unit simulator[C]. '11 National simulation technology academic conference proceeding: p. 286-289(2011)

Improved Ant Colony Algorithm base on Slab Cluster for Roll Planning

Helan Liang^{1, a}, Jie Zhang² and Bo Hu¹

¹ Department of Logistics Engineering, School of Mechanical Engineering, University of Science and Technology Beijing, Beijing, 100083, China

² Department of Mechanism Engineering, School of Mechanical Engineering, University of Science and Technology Beijing, Beijing, 100083, China

^alianghelan@gmail.com

Keywords: Roll planning; Slab cluster; Ant colony algorithm

Abstract. Focusing on the disadvantages of recent researches for roll planning that seldom consider the warm-up part and solution efficiency is low, in this paper, a parallel planning model and an improved ant colony algorithm were proposed to solve the problem. Firstly, the model considering constraints of both warm-up part and staple one was designed; Secondly, the improved ant colony algorithm was proposed where the slab cluster was used to decrease the searching scope and the local optimization to improve the efficiency of pheromone accumulation. Finally, with production data from hot strip mill, we proof the method can get the best results by comparing with other two ant colony algorithms.

Introduction

Planning and scheduling is the critical issues of hot rolling production in steel industries which has been widely studied [1-8]. Up to date, further researches on the planning of hot strip mills are needed as follows: 1) most researches are focus on the serial solving of rolling problem. The algorithm is simple and easy to implement, but the problem is the plan made first is good while the last become worse. 2) Constraints of warm-up parts of the rolling plans haven't been considered expect reference [3] whose rolling model was simplified. As the warm-up parts have special requirements to materials, it should not be ignored. 3) As there are lots of candidate slabs in the yards, the scale of the problem becomes even larger when it comes to parallel planning. Considering the disadvantages of recently researches, a parallel multiple-benefits planning model for planning of hot rolling mills is proposed. The model considers both the warm-up part and staple part, and the slab cluster method is designed according to the characteristics of slabs. Further, an ant colony algorithm based on slab cluster is proposed for problem solving. Finally, simulation with production data is used for model validation.

Description of the problem

The problem of rolling planning is to schedule the rolling batches according to the process restraint and optimization goals of hot rolling. Usually, the width of the rolling coils in a rolling unit has a coffin structure as Fig. 1 shown.

The constraints are as follows: 1) the constraints of warm-up materials: (a) restrictions on the length; (b) restrictions on the range as the width increase; (c) the hardness of coiled sheet should not be too large and the range of hardness change should be small; (d) the change range of thickness should be small; (e) contract of the high surface quality can not be assigned; 2) the restrict of staple materials: (a) restrictions on the length; (b) changes in the width should be non-growth direction; (c) changes of thickness, hardness should be

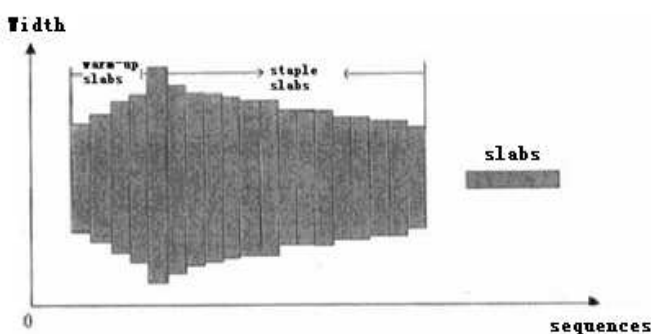


Fig.1 width Structure of a rolling plan

smooth; (d) continuous rolling of the same width (or 50mm width) slab can not exceed a certain length; (e) contract of the most high surface quality can only be rolled within a certain number of rolling kilometers. The goals are as follows: 1) Maximize the total rolling length of the sequence; 2) Minimized the total punishment which is caused by the width, thickness, hardness and temperature jump.

Mathematical models

This paper introduces virtual slab 0 as the starting and ending of the slab and converts the problem of the parallel constraints of roll planning to the Multi-price VRP model. The variables and parameters in the model are defined as follows:

x_{ij}^k, y_i^{kt} are decision variables:

$$x_{ij}^k = \begin{cases} 1 & \text{in the } k\text{-th rolling unit, slab } i \text{ is followed by slab } j, \\ & i, j = 0, 1, 2, \dots, N, \text{ and } i \neq j; k = 1, 2, \dots, K \\ 0 & \text{else} \end{cases}, \quad y_i^{kt} = \begin{cases} 1 & \text{slab } i \text{ is in the } t\text{-th area of the } k\text{-th rolling unit} \\ & i = 0, 1, 2, \dots, N; t = 1, 2; k = 1, 2, \dots, K \\ 0 & \text{else} \end{cases}$$

tp_i is used to define whether slab i can be used as warm-up material; p_i represents the value of slab i . It is a function related to the rolling length, priority and delivery.

b_{ij} represents the costs if slab i produced after slab j . it is a function related to the costs of the rolling width, thickness and hardness respectively of adjacent slabs.

L'_{\max}, L'_{\min} are the maximum, minimum of the total length of the strip rolling of the t -th rolling area $t, t=1, 2$;

z_{ij}, fz_{ij} reflect whether slab i and slab j have the same width or continuous rolled within the range of 50mm;

Sl_{\max}, Fl_{\max} represent the maximum length of continuous rolling under the same width or within the range of 50mm in the rolling unit.

The mathematical model of this problem is defined as follows:

$$\min X = W - \sum_{k=1}^K \left(\sum_{i=1}^N \sum_{t=1}^2 p_i y_i^{kt} - \sum_{i=1}^N \sum_{j=1}^N b_{ij} x_{ij}^k \right) \quad (1)$$

$$\text{s.t. } \sum_{k=1}^K \sum_{t=1}^2 y_i^{kt} \leq 1 \quad i=1, 2, \dots, N \quad (2)$$

$$\sum_{t=1}^2 y_0^{kt} = 1 \quad k=1, 2, \dots, K \quad (3)$$

$$\sum_{j=0}^N x_{ij}^k = \sum_{t=1}^2 y_i^{kt} \quad i=1, 2, \dots, N; k=1, 2, \dots, K \quad (4)$$

$$\sum_{i=0}^N x_{ij}^k = \sum_{t=1}^2 y_j^{kt} \quad j=1, 2, \dots, N; k=1, 2, \dots, K \quad (5)$$

$$L'_{\min} \leq \sum_{i=1}^N y_i^{kt} l_i \leq L'_{\max} \quad t=1, 2; k=1, 2, \dots, K \quad (6)$$

$$\sum_{j=1}^N z_{ij} l_j \leq SL_{\max} \quad i=1, 2, \dots, N \quad (7)$$

$$\sum_{j=1}^N fz_{ij} l_j \leq FL_{\max} \quad i=1, 2, \dots, N \quad (8)$$

Whereas, the objective function (1) maximize the total revenue, W is a large number; Constraints (2) ensures that slab i can only be planed for one time; Constraints (3) defines that each unit contains a virtual rolling slab 0; Constraints (4), (5) ensure that there is only one slab j rolled after slab i ; Constraints (6) is the total rolling length constraint of warm-up materials and staple ones; Constraints (7), (8) are the length constraint of the width of the staples and 50mm width-rolling.

Model Solutions

In this paper, an ant colony system base on slab cluster method is designed. The entire ant colony is divided into M groups each with K ants. Ants are united into groups when parading, and start from the K virtual nodes.

Algorithm design

Definition of slab cluster

In the actual production, many rolling materials have similar dimensions and physical properties, such as: rolling specifications, quality requirements of surface, and slabs with similar feature mentioned above can be replaced during the production process. Considering the above features, in this paper, we defines the slab cluster according to which slabs with the same steel, rolled specifications, surface quality requirements and similar heating temperature, delivery time, order priority are classified into one cluster. Such slab cluster is used as the virtual slabs during the node selection and the updating of the pheromone, so to reduce the solving scale.

Sequence selection strategy

"From the inside out" strategy is used when choosing the next node of the warm-up parts. That means start from the staple initial slab of the rolling unit, warm-up materials are be chosen first to build up the inverted confined shape of the plans. After all warm-up constraints are satisfied, arrange the nodes of the staple parts forwardly.

Before selecting the next node, the slab cluster should be chosen firstly. Ants will choose the slab which has the maximum transition probability as the next node by probability Q_1 as the Eq. 9 shows, and choose by the probability of $1-Q_1$ at random,. After the slab cluster is decided, choose one slab randomly in the corresponding slab cluster as the next node.

$$j = \arg \text{Max}[\tau_{ij}(t)]^\alpha * [\eta_{ij}]^\beta \quad q_1 \leq Q_1 \quad j \in Z \quad (9)$$

Whereas, i, j are the present and the next slab cluster respectively. $\tau_{ij}(t)$ is the pheromone concentration which is connected to arc(i, j) in the t th generation; $\eta_{ij} = p_j / (0.1 + b_{ij})$ represents the expectation of the ant to convert from cluster i to cluster j , α represents the relative importance of the arc; β represents the relative importance of η_{ij} ; q_1 is a decimal generated randomly; Q_1 is the pre-set threshold; Z is set of the candidate slab clusters which satisfied the constraint.

Local optimization strategy

In this paper, local optimization strategy is designed to optimize the path of the ant colony so to accumulate the pheromone more efficiently. Considering the solutions may not become better if only adjustment of single slab is applied because constraints to adjacent slabs are similar in one unit. Therefore, in this paper adjustment strategy is designed not only for single slab, but also for continuous slab segment including: insert a single slab (or slab zone), exchange of a single slab (or slab zone), delete a single slab (or slab zone), and adjust the sequence. Whereas, the first three strategies is the optimization operators between rolling units while the fourth is within one unit. Once the income of the adjacent slab in a rolling unit is less than the threshold, run the optimize operation. Repeat until the number of consecutive non-improving solutions of the optimal solution is greater than the local non-threshold Q_2 , and then jump out of the local optimization process.

Pheromone update

The strategy integration of global path update and local path update are applied in this paper, which is as shown in Eq. 10. Compare the contemporary optimal solution L_{ib} and the optimal solution of all the iterations L_{gb} firstly after each iteration. Update the pheromone whose visibility weight is large enough between the slabs in the contemporary optimal circuit, otherwise, don't execute the update.

$$\tau_{ij}(t+1) = (1 - \rho)\tau_{ij}(t) + \frac{L^{gb}}{L^{ib} * L^{ib}} * \frac{\eta_{ij}}{d_i} \quad (i,j) \in T_{ib}, L^{ib} \leq Q_3 * L^{gb}, \eta_{ij} \geq d_i \quad (10)$$

Whereas, T_{ib} , L_{ib} are the optimal circuit of contemporary generation and its target; L_{gb} is the optimal value for all cycles; ρ is the evaporation coefficient; η_{ij} is the visibility of adjacent nodes which is corresponding to the cluster (i,j) in the path; d_i is the pre-set visibility threshold value; Q_3 is the pheromone update threshold value.

Process Description

- Step1: Input slabs data; Initialize the parameters; $g=1$;
- Step2: Ants in each group execute the g th generation cruise;
- Step3: Compare the travel costs of ants in each group; get the optimum circuit T_{ib} of the g -th generation;
- Step4: Optimize T_{ib} according to the local optimization strategy;
- Step5: Update the pheromone according to the Pheromone update strategy;
- Step6: If $g < G$, update $g=g+1$, go to Step2; else, output the optimal solution.

Model validations

To validate the algorithm mentioned above, production data with 1300 slabs from one hot strip mill are used. Firstly, 205 slab clusters are defined. Running 10 times independent operations and the average results are shown in Table 1.

Table1 The simulation results

Algo-rithm	average warm-up parts (km)	length of average staple parts (km)	length of Average costs	penalty	Computation time (s)
1*	6.41	82.35	3607		2992
2*	6.48	89.61	3158		3213
3*	6.34	89.93	3135		449

* 1: standard ant colony algorithm; 2: ant colony algorithm with local optimization; 3: ant colony algorithm with local optimization based on slab cluster

As is shown in table1, the solution speed of the standard ant colony algorithm is slow because pheromones are too scattered and the efficiency is the worst; The solution result of the ant colony algorithm with local optimization is better, but the speed is slow; The best results can be received by the method we proposed, as the search scale of the ant colony algorithm is 15.7% of the original problem thanks to the slab cluster; What's more, the local optimization greatly improves the accumulation speed of pheromone.

Change of with and thickness in a rolling unit is shown in figure2. We can see the solving result is feasible. In addition, calculate the usage times of the four partial optimization strategies we proposed when running the algorithm. From figure3 we can see the four partial optimization strategies are all used when optimizing, especially, inserts and exchange strategies are used much more frequently. Comparing the adjustment of the single slab to the slab section, adjustment of the slab section plays an important role in the optimization process.

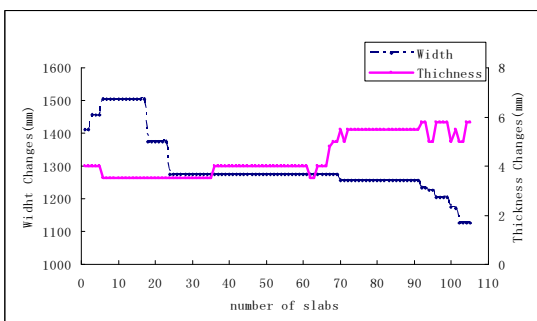


Fig.2. Change of with and thickness in a unit

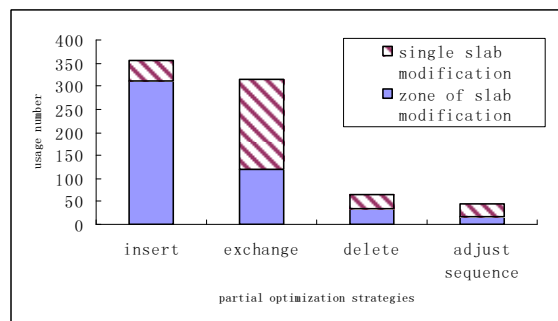


Fig.3. Usage times of partial optimization strategies

Conclusions

This paper proposes a parallel multiple-benefits model for the roll planning, and use the method of the ant colony algorithm with local optimization based on slab cluster to solve the problem. Conclusions are as follows:

This model not only considers the conventional constraints of the staple material but also consider the planning of the warm-up materials, so to make the model more comprehensive;

To increase the solution efficiency, this paper proposes a hybrid ant colony algorithm base on the slab cluster method and the local optimization strategies which can adjust both the single slab and continuous slab segment;

Production data are used for validation. Comparing with other two algorithms, the method we proposed is best as it reduces the candidate slabs to 15.7% of the original problem and the solution speed improves significantly thanks to the slab cluster and local optimization strategies.

References

- [1] Lopez L, Carter W M, Gendreau M. The hot strip mill production scheduling problem: A tabu search approach [J]. *European Journal of Operational Research*. 1998,106: 317~ 335.
- [2] Peter Cowling, Wafa Rezig. Integration of continuous caster and hot strip mill planning for steel production [J]. *Journal of Research and Development*. 2000, (3): 185~208.
- [3] Li Yao-hua, Wang Wei, Xu Le-jiang. Rolling plan model and algorithm in hot rolling plant [J]. *Control and Decision*, 2005,20(3): 275~279.
- [4] Chen Ai-ling, Yang Gen-ke, WU Zhi-ming. Rolling Plan Optimization Model and Algorithm for Hot Rolling Processes; *Journal of System Engineer* [J]. 2006,18(09): 2484~2562.
- [5] Gao Huimin, Zeng Jianchao. Interlegent scheduling theory and application in steel industries [M]. *Metallurgical Industry press*. 2006:10.
- [6] Sun Ling, Li Tie-ke. Constraint satisfaction algorithm of batch planning for steel making-continuous casting-hot rolling [J]. *Computer Integrated Manufacturing Systems*, 2007,13(5): 110~114.
- [7] ZhaoJun, Wang Wei, Pan Xuedong. Parallel particle swarm algorithm and its application in hot rolling planning [J]. *Computer Integrated Manufacturing Systems*, 2007, 13(4): 698-703.
- [8] Liu Shi-xin, Song Jian-hai. Model and algorithm for solving hot strip rolling batch planning problems [J]. *Control Theory & Applications*, 2007, 24(2): 243-248.

Study on Performance Optimization of Car Diesel Engine with VNT Based on One-dimensional Simulation and Experimental Verification

Lianxu Wang^{1, a}, Dawei Qu^{2, b}, Changqing Song^{3, c}, Ye Tian^{4, d}

^{1,2,3,4}State Key Laboratory of Automotive Simulation and Control, Jilin University

^{1,2,3,4}5988 Renmin Street, Changchun, Jilin, P.R.China

^awanglianxu2006@126.com, ^b14128274@qq.com, ^c344766032@qq.com, ^d723687352@qq.com

Keywords: car diesel engine, one-dimensional simulation, VNT, compression ratio, distribution phase

Abstract. To research the performance optimization of high speed car diesel engine, firstly according to the characteristic of car diesel engine with Variable Nozzle Turbocharger (VNT), one-dimensional cycle model of the engine was established by using simulation software BOOST and validated by experimental data in this paper. The turbine blades' opening corresponding to different speed was determined. Therefore the problem that the VNT surges at low engine speed and the inlet air flow is insufficient at high speed was solved. Based on the above model, this paper improved the efficiency of the engine by optimizing the compression ratio and the distribution phase of camshaft and then used the experimental data to check the simulation results. Meanwhile the fuel consumption and the possibility of the engine operation roughness decreased.

Introduction

With continuous development of Vehicle industry, diesel power of car has become an inevitable trend. In recent years the ratio of diesel cars increased to more than 50% in Europe and the ratio is increasing greatly year by year in America and Japan. Domestic automobile manufacturers still have not given up the development of diesel cars as DI diesel engine has tremendous development potential on power, economy and low emissions indicators. The variable swallowing capacity turbocharger becomes essential technology to cope with emission regulations and to decrease fuel consumption, while meeting the demand for increasing engine power output. A turbocharger with new structure has been developed for car diesel engines, the Variable Nozzle Turbocharger (VNT). The object of VNT is to improve engine performance, over a broad engine speed range, by changing the swallowing capacity of turbine with variable nozzles blades. In this paper, we set up a VNT car diesel engine model by using AVL BOOST one-dimensional simulation software, and optimized the performance of the engine by comparing the simulation computed results and bench experimental results.

Building and Validating One-dimensional Simulation Model

Description of Test Prototype Parameters

Table 1. The Parameter of Experimental Prototype

Item	Specification	Instruction
Number of cylinders	4	
Cylinder diameter × stroke	78X138	Unit[mm]
Displacement	1.796	Unit[L]
Rated power / speed	80.9[kW]/4000[rpm]	
The maximum torque /speed	239.6[N·m]/2200-2600[rpm]	
Aspirated mode	VNT	Air Cooling

Test prototype is a four-cylinder high speed DI diesel engine with VNT which meets Europe IV emission standard. The technologies of variable nozzle turbocharger and exhaust gas recirculation are adopted. Specific parameters are given by the above Table 1.

The Overall Constitution of The Model

The established model consists of a VNT and intercooler, EGR valve and EGR intercooler and so on. Based on the actual configurations of the engine and related parameters contain structure, environment, combustion, heat transfer parameters and so on, we set up the one-dimensional simulation model (Figure 1). The combustion model is single Vibe model and combustion parameters (start angle of combustion, combustion duration angle, combustion shape m and heat release rate) are calculated by BURN Function according to the measured parameters such as cylinder pressure, environment conditions, distribution phase and injection quantity. The introduction of model constitutes is given in Table 2.

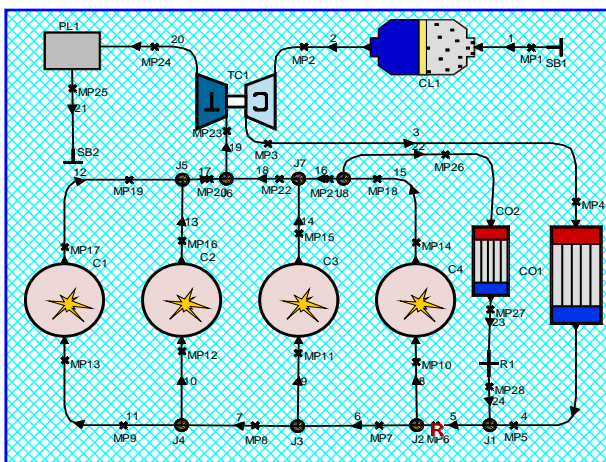


Fig.1. One-dimensional model

Table 2. Model components

Element	Instruction
SB1	System boundary (iIntake)
CL1	Air Filter
TC1	VNT
CO1	Intercooler
CO2	EGR intercooler
R1	EGR control valve
PL1	Volume chamber
C1~C4	Cylinder
MP1~MP25	Measuring points
SB2	System boundary (exhaust)
The rest	Pipeline

It is noteworthy that the calculate model of the turbocharger turbine is full model. Therefore compressor full characteristic map need to be input into the simulation model. To the actual compressor rotate speed and flow can be reflected exactly in different external environments (pressure and temperature), the corrected rotate speed and flow are used to the map. The VNT compressor map is shown in Figure 2. About the turbine map, there are totally seven maps distinguished by turbine blades opening as follow: 0.083, 0.17, 0.33, 0.5, 0.67, 0.83,1. Because of limited space, this paper only shows the map about the turbine blades opening completely (Figure3 and 4).

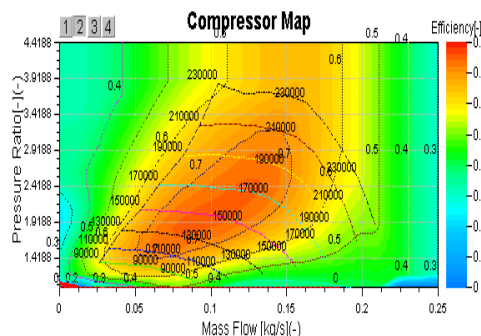


Fig.2. The VNT compressor full characteristic map

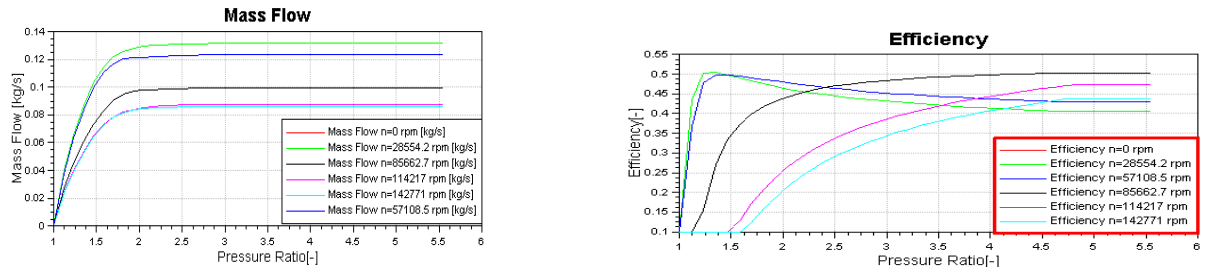


Fig.3 and 4. The VNT turbine characteristic map

The opening of the turbine blades corresponding to different speed is determined on the basis of the VNT map. The problem that the VNT surges at low engine speed and the inlet air flow is insufficient under the condition of high speed is solved.

Model Verification

When simulation software is used to study engine characteristic the key is the reliability of the model. In this paper we verified and modified the model parameters corresponding to different operation conditions through the advanced experimental data of the test prototype after establishing the whole engine model. Comparison of experimental data and simulation data is shown in Table 3. The results show that the simulation model is reliable and exact. And then we can use this engine model to optimize the parameters affecting the performance of car diesel engine.

Table 3. Comparison of experimental data and simulation data

Rotate speed [rpm]	Data resource	Torque [N·m]	Intake most flow [kg/h]	Intake gas pressure [kPa]	BSFC [g/kw·h]	Pressure rario [-]
2400	Experiment	239.6	247	212.7	205.1	2.108
	Simulation	242.2	260.4	208.8	202.9	2.100
1000	Experiment	140.5	64	117.8	243.8	1.175
	Simulation	141.0	61	114.6	234.7	1.136
4000	Experiment	192.8	440	225.8	254.9	2.238
	Simulation	206.8	439.7	233.4	232.7	2.378

Optimizing The Compression Ratio

Firstly it's noted that all the operation conditions we simulated are full-load in this paper. Compression ratio could affect gas exchange process, thermodynamic process and combustible quality of the engine. This paper optimized the compression ratio of VNT car diesel engine by the comparison between simulation and experimental results.

The Analysis of Simulation Results

Compression ratio changes from 17 to 20 (intervals 0.5) on the premise of remaining the fuel injection quantity, combustion parameters (start angle of combustion, combustion duration angle and combustion shape m) and the other parameters unchanging. The power and the volumetric efficiency of engine do not change significantly as the compression ratio increases. Because of the stronger vortex and turbulence generated in the compression process, speeding up the burning speed of engine, reducing the heat, the fuel consumption decreases with the increase of the compression ratio (Figure 5). The exhaust gas temperature also decreases distinctly with the increase of the compression ratio (Figure 6) and on the contrary the peak firing pressure increases 20 bar (Figure 7). So the compression ratio should not be too high. Otherwise the engine will work rough.

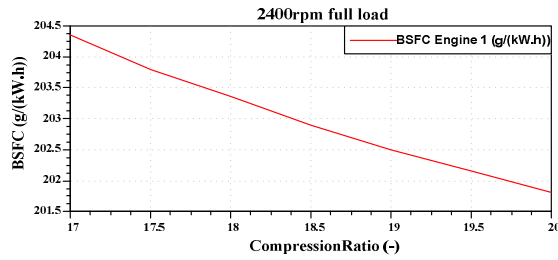


Fig.5. The compression ratio impact on fuel consumption exhaust

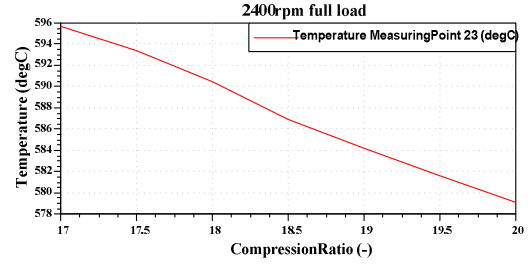


Fig. 6. The compression ratio impact on gas temperature

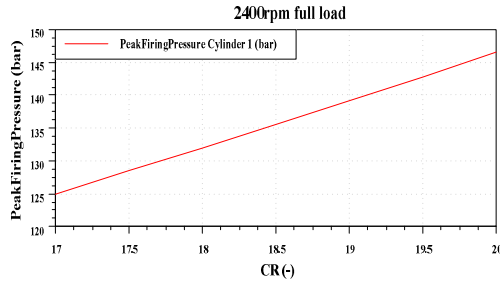


Fig.7. The compression ratio impact on peak firing pressure

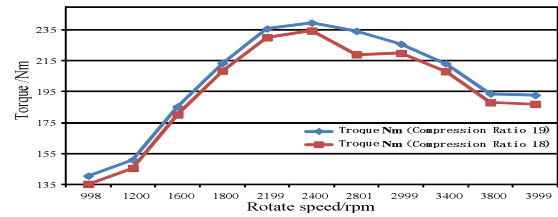


Fig.8. Test Performance comparison curve in the compression ratio of 18 & 19

Experimental Validation of Simulation Results

In the process of experimental validation of simulation results, we compared the experimental performance of engine under the compression ratio of 18 and 19. As shown in Figure 8 the test results show that the engine power improves and fuel consumption decreases with increasing the compression ratio. Finally according to the simulation and experimental results, compression ratio between 18 and 19 is desirable.

Optimizing The Distribution Phase

In the optimization design process, the more the optimization variable, the better the optimization effects. But the workload will increase. In order to reduce the time we selected three typical operating conditions under external characteristics as follows: calibration condition (4000rpm), the maximum torque condition (2400rpm) and low speed condition (1000rpm). The distribution phase is successively optimized, that is at first we optimized the exhaust valve advance open-angle which is indicated as EVO in BOOST software. The variation of EVO changes between -20 degrees and 20 degrees on the basis of the original EVO (Figure 9 to 12, the negative direction of X-axis represents increase). Subsequently the intake and exhaust valves overlap angle is modified which is indicated as the sum of IVO (intake valve early open-angle) and EVC (exhaust valve late close-angle). In the process of the overlap angle the variation of IVO changes between -10 degrees and 10 degrees on the basis of the original IVO on the premise of remaining the EVC unchanging (Figure 13 to 16, the negative direction of X-axis represents increase). The original distribution phase is as follows: EVC is 23 degrees, EVO is 53 degrees, IVC is 56 degrees and IVO is 8 degrees.

Optimizing The Exhaust Advance Angle

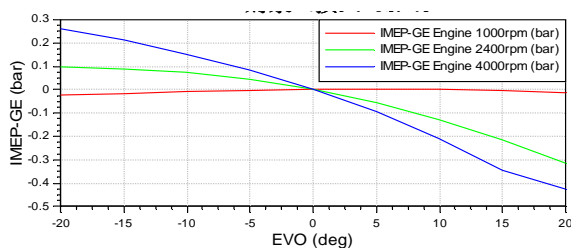


Fig. 9. The effects of EVO on pumping losses

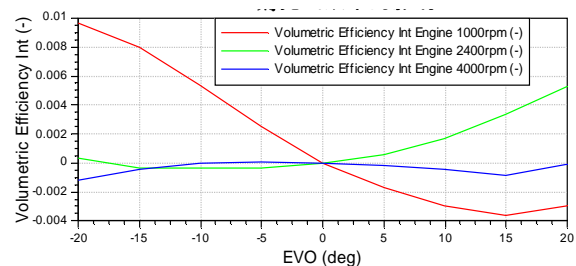


Fig.10. The effects of EVO on volumetric efficiency

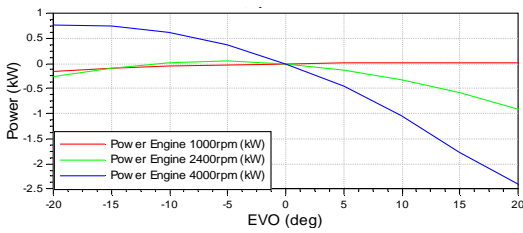


Fig. 11. The effects of EVO on power

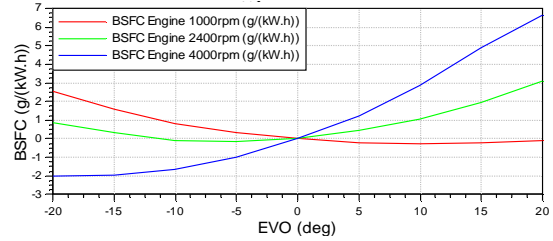


Fig. 12. The effects of EVO on fuel consumption

As shown in Figure 9 (the negative direction of X-axis represents increase), increasing the exhaust advance angle reduces the pumping losses in high and medium speed. However the volumetric efficiency increases (Figure 10). We can know that the best exhaust valve advance open-angle correspondind to the maximum power is different under the conditions of different engine speed (Figure 11). The engine will drastically reduce and the fuel consumption increase with continuous the reduction of EVO in the case of EVO is lower than 48 degrees (Figure 11 and 12). In order to make the engine have good performance under all conditions, we determined that the EVO is 48 degrees by comprehensive consideration.

Optimizing The Intake and Exhaust Valve Overlap Angle

As mentioned above, the optimized EVO is 48 degrees and EVC remains the original 23 degrees. By the analysis of Figure 13, it's seen that fuel consumption at medium and low speed changes a little with the change of intake and exhaust valves overlap angle. But fuel consumption at full speed changes significantly. As the engine work rarely under calibration condition, we can consider secondly the influence of overlap angle on the full speed performance. The pumping losses increases with the overlap angle decreasing. And then the overlap angle corresponding to the optimal value of volumetric efficiency at different speed is different. As shown in Figure 16, when the overlap angle is less than 35degrees decreasing the overlap angle reduces the engine power at medium speed obviously. From Figure 13 to 16, we can see that the effects of the overlap angle on the performance at low speed are not significant. Generally speaking, we think it's reasonable that the overlap angle is between 25 degrees and 35 degrees.

Finally the overlap angle is determined as 35 degrees namely that IVO is 12 degrees and EVC is 23 degrees by comparing experimental data at 35 degrees and 25 degrees overlap angle. The optimized distribution phase is as follows: EVC is 23 degrees, EVO is 48 degrees, IVC is 56 degrees and IVO is 12 degrees.

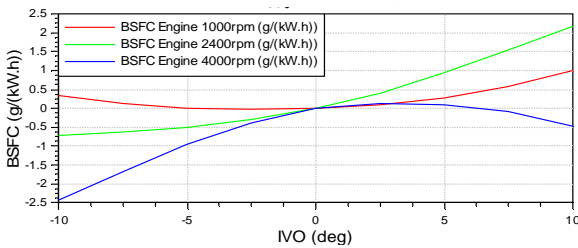


Fig.13. The effects of IVO on fuel consumption

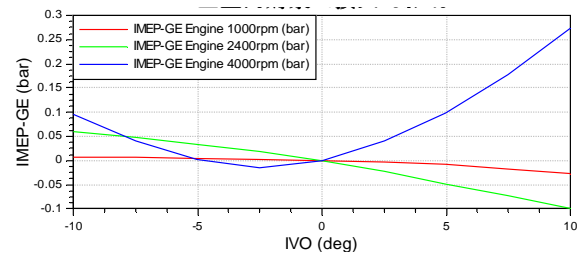


Fig.14. The effects of IVO on pumping losses

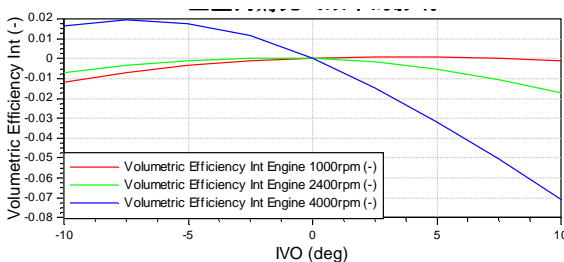


Fig. 15. The effects of IVO on volumetric efficiency

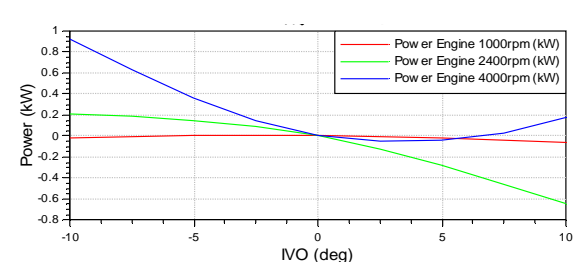


Fig.16. The effects of IVO on power

Summary

According to the working principle of diesel engine and modular features of BOOST, this paper builds the model of the four-cylinder high speed DI diesel engine with VNT which meets Europe IV emission standard and makes use of the validated model to optimize the parameters affecting the performance of the engine. The research includes as follows:

Combustion parameters about single Vibe model are calculated by BURN function according to the advance experimental data. We used these parameters to set up the simulation model and obtained the results very close to the experimental data;

Based on the full characteristic map of VNT, we determined the opening of the turbine blades corresponding to different operation conditions. The problem is avoided that VNT cannot be matched with the engine;

After checking the effectiveness of the calculation model, the model is used to improve the efficiency of engine by optimizing compression and distribution phase. And then the simulation data is validated by comparing to the test data. That proved that the simulation model is reliable and we can do further research on improving the performance on the basis of this simulation model.

References

- [1] N.Guerrassi, P.Dupraz. A Common Rail Injection System for High-Speed Direct Injection Diesel Engines, SAE paper, 980803.
- [2] Yohan Chi, Jaehoon Cheong, Changho Kim. Effects of VGT and Injection Parameters on Performance of HSDI Diesel Engine with Common Rail FIE System. SAE paper, 2002-01-0504.
- [3] Steven Arnold. Turbocharging Technologies to Meet Critical Performance Demands of Ultra-Low Emissions Diesel Engines. SAE paper, 1999-01-1359.
- [4] Maktoto Hagashi. Development of a Turbocharging System with Variable Area Turbine Nozzle for HD Trucks. SAE paper, 920045.
- [5] Steve Arnold, Mark Groskreutz. Advanced Variable Geometry Turbocharger for Diesel Engine Applications. SAE paper, 2002-01-161

A Simple Linear Discrimination Algorithm for AD Patients and Normal Controls

Yunyi Yan^{1,a}, Guozhang Hu^{2,b}, Baolong Guo^{1,c}, Yujie He^{1,d}

¹ ICIE Institute of Electro-mechanical Engineering School, Xidian University, Xi'an, 710071, P.R. China

² Department of Neurosurgery, China-Japan Union Hospital, Jilin University, Changchun, 130033 P.R. China

^ayyyan@xidian.edu.cn, ^bhuguo Zhang_4266@sina.com, ^cblguo@xidian.edu.cn, ^dheyujie0702@126.com

Keywords: Linear Discrimination, Alzheimer's disease, cortical thickness, Parameter Optimization

Abstract. One simple but effective discrimination method was presented in this paper to separate AD from normal controls. After detecting the thickness of cortex with highly significant difference, the mean and standard deviation of these vertices are computed to construct confidence intervals. We introduced one relax coefficients to control the width of intervals and by experiments the coefficients was optimized. Experiments results showed that using this simple method, the classification accuracy, sensitivity and specificity of Alzheimer's disease versus normal controls could be as high as 85%, 88.89% and 93.84% respectively.

Introduction

Alzheimer's disease (AD) has been thought as one of the most important older people disease, for its serious effect and popularity. The cause and progression of Alzheimer's disease are not well understood. And the diagnose or classification of AD is still one hot spot in medicine and engineering fields.

Cortical thickness has significant advantages in terms of precision and interpretability over voxel-based morphometry [1]. And in many cases, cortical thickness is thought as one important criteria for disease detection, such as Parkinson's disease (PD)[2], and ageing-related diseases [3].

There are many methods to classify the patients with controls. For example, one multivariate analysis in volume is proposed in [6], and multimodal classification using linear support vector machine[7]. But most of these methods are very complicated and difficult to use for doctors. And in most standard medicine image processing pipeline, such as FreeSurfer [4], the cortical thickness is standardized and easy to compute.

Methods and algorithms

Sample data set. The sample data set we use in the study is the cerebral cortical thickness data extracting from magnetic resonance image (MRI) of 199 AD patients and 227 normal subjects, and 40% of that is used as training set (80 AD patients, 91 normal subjects), 30% of that is used as validation set(60 AD patients ,68 normal subjects),the other is used as test set(59 AD patients,68 normal subjects). The brain of every AD patient or normal subject is divided into left hemisphere and right hemisphere and there are 40962 cerebral cortical thickness data for every hemisphere.

In addition, all AD patients and normal subjects have corresponding demographic data (age, gender). The data were collected from ADNI (<http://adni.loni.ucla.edu/>). The thickness value was calculated by FreeSurfer [4].

Statistical Models. During the study, the statistical analysis is accomplished by SurfStat, a statistical toolbox [5] created for MATLAB7 (The MathWorks, Inc.) by Dr. Keith Worsley (<http://www.math.mcgill.ca/keith/surfstat/>).

For 80 AD patients(AD group) in training set, there are 41 male patients and 39 female patients, and the average age is (75.44 ± 6.93) years old, For 91 normal subjects(control group) in training set, the male is 53 and the female is 38 ,the average age is (76.45 ± 5.57) years old, what's more, there are no significant differences for age($P=0.1483$) and gender($P=0.1811$) between AD group and control group.

Since the specificity of each individual sample is significant, we use SurfStatNorm to normalize the cortical thickness data and reduce the differences between individual samples, each vertex of each sample gets a new cortical thickness data by subtracting the global mean. After that we convert age, gender and group to terms (Age, Gender, and Group) that can be combined into a multiple linear regression model as follows:

$$Y \sim b_0 + b_1Age + b_2Gender + b_3Group + e \quad (1)$$

And use SurfStatLinMod to fit the Multiple linear regression model and estimate the coefficients $[b_0, b_1, b_2, b_3]$, then we specify a group contrast (contrast = Group.normal - Group.AD) for testing the cortical thickness difference between AD group and control group with controlling for demographic factors(age gender) and calculate the T-statistic, the T-statistic values for all mesh vertices produce a T-statistic map which is shown in Fig.1.

And after converting T-statistic values corresponding to P-statistic values for all mesh vertices, we get the corrected P-statistic values, which are corrected by family wise error (FWE) method in SurfStat. The FWE value is the false positives rate for all mesh vertices where the t-value is above the selected threshold.

Setting the threshold to an FWE of 0.05, so only if P-statistic value is less than 0.05, the result is statistically significant, and the smaller P-statistic value, the more significant result. For each mesh vertex, only if P-statistic value is larger than 0.05, the cortical thickness difference between AD group and control group cannot be seen as statistically significant.

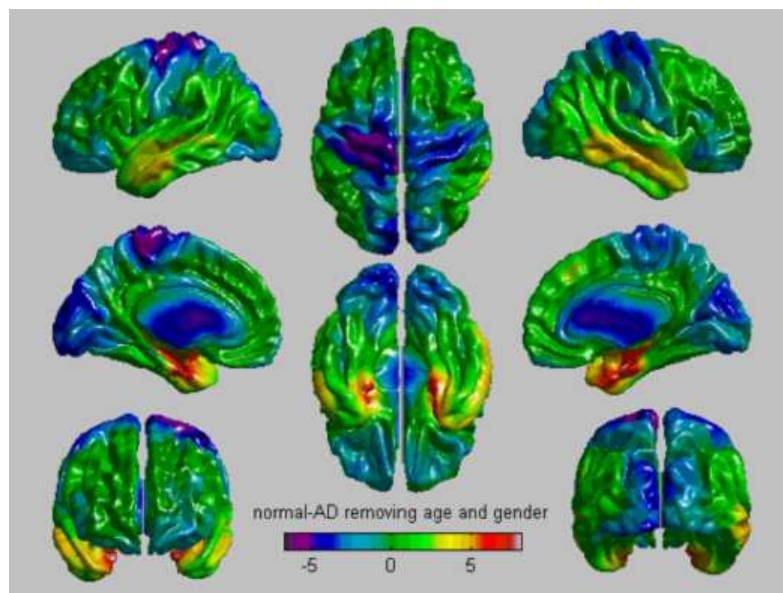


Fig.1. The results of T-statistic values of Cortical Thickness regressed against group for all mesh vertices

Because the cerebral cortical thickness data extracting from magnetic resonance image (MRI) has been registering and re-sampling, in each hemisphere each mesh vertex has a corresponding index number and each index number has a corresponding label number in AAL template[8] and the label number has a corresponding description of the region where the vertex is located, we can find the index number and the corresponding label number and the corresponding brain region of the mesh vertex whose cerebral thickness difference between two groups is statistically significant for each hemisphere.(See Table1)

Table1. The vertices with high significant difference in cortical surface.

Region Label	Significant vertices	Corresponding brain region
29	1	Left Insula
39	282	Left Parahippocampal gyrus
81	45	Left Superior temporal gyrus
83	153	Left Temporal pole: superior temporal gyrus
85	9	Left Middle temporal gyrus
87	8	Left Temporal pole: middle temporal gyrus
40	434	Right Parahippocampal gyrus
56	30	Right Fusiform gyrus
82	190	Right Superior temporal gyrus
84	219	Right Temporal pole: superior temporal gyrus
86	335	Right Middle temporal gyrus
88	56	Right Temporal pole: middle temporal gyrus
90	26	Right Inferior temporal gyrus

Discrimination algorithm. We take the characteristic of significant difference of cerebral cortical thickness of these mesh vertices between two groups as our basis for the discrimination between AD patients and normal subjects, and hypothesis testing method is used to achieve it.

As the new cortical thickness data of each vertex of all samples in training set is of normal distribution, firstly, we need obtain the average (μ) and standard deviation (ϕ) of the new cortical thickness of each vertex of all AD patients and normal subjects of training set respectively.

Secondly, setting confidence interval to $(\mu \pm a\phi)$ for AD patients and for normal subjects (coefficient a is used to the optimization of confidence interval). When coefficient a is determined, if the thickness data of the majority of the vertex fall into the confidence interval of AD patients, the sample is judged to AD patient, otherwise the sample is judged to be normal.

Thirdly, validation set is used to find the optimal value of coefficient, that is to say, the optimal confidence interval is determined, which can achieve the best discrimination between AD patients and normal subjects. In the process of finding the optimal value of coefficient, we need make a relatively large step size (the step size is one here) based on $a=1.96$ and the accuracy was computed by increasing or decreasing step, so we could determine the direction of adjustment for coefficient a and eventually find the optimal coefficient. Judging from the experimental results, the optimal value of coefficient and the optimal confidence interval is set to around 4.30, which was used to discriminate between AD patients and normal subjects in testing set.

Experimental Results

It can be seen from Fig.1 and Table1 that the significantly different foci of the thickness of cerebral cortex between AD patients and normal subjects are mainly located in the temporal lobe and parahippocampal gyrus regions of both hemispheres. Parahippocampal gyrus is the most important area of the brain with episodic memory-related function.

Parameter Optimization. For coefficient a , when $a=1.96$, the result of discrimination between AD patients and normal subjects in validation set is in Table2. From Table2, we can see that the error rate is 60% for AD patients and is 0 for normal subjects. Apparently, though all the normal controls are classified correctly, yet the error rate is 60% for AD patients is too large. To improve the classification accuracy, the parameter a needs optimizing.

Table2. The statistical result of discrimination in validation set when $a = 1.96$

	AD patients	Normal controls (NC ₊)
AD patients (AD _T)	24 (AD ₊)	36 (AD.)
Normal controls (NC _T)	0 (NC.)	68 (NC ₊)

In the process of the adjustment of coefficient a , we increase one each time coarsely. When $a=4.96$, inflection point of the result of discrimination occurs, so we make small adjustment for coefficient a between 3.96 and 4.96. Then, we reduced the step size to 0.1 so that the optimal point won't be missed. Eventually, if the a value is set to around 4.30, the result of discrimination got to the best. The Table 3 listed the results. The error rate is 6.67% for AD patients and 10.29% for normal subjects, so the median 4.30 is the optimal value of coefficient a .

Table3. The statistical result of discrimination in validation set when $a=4.30$

	AD patients	Normal controls (NC ₊)
AD patients (AD _T)	56 (AD ₊)	4 (AD)
Normal controls (NC _T)	7 (NC ₋)	61 (NC ₊)

Performance Comparison. For testing set, when coefficient a is the optimal value $a=4.30$, the result of discrimination between AD patients and normal subjects is 49 out of 59 (for AD) and 59 out of 68 (for normal controls), the total accuracy is 85.04%. We compared the accuracy with recently proposed methods, including volume multivariate's analysis in volume[6], and multimodal classification using linear support vector machine[9]. Table 4 listed the performance comparison with other two recent papers. The involved three criteria were defined as:

$$\text{Accuracy} = (\text{AD}_+ + \text{NC}_+)/(\text{AD}_T + \text{NC}_T) \times 100\% \quad (2)$$

$$\text{Sensitivity} = \text{AD}_+ / (\text{AD}_+ + \text{NC}_-) \times 100\% \quad (3)$$

$$\text{Specificity} = \text{NC}_+ / (\text{AD}_- + \text{NC}_+) \times 100\% \quad (4)$$

Table 4. Performance of data set and the comparison with other algorithms.

	Proposed method	MNI Volume method in[6]	MRI+PET method in[9]
Accuracy	85.04%	84.21%	87.60%
Sensitivity	88.89%	81.00%	78.90%
Specificity	93.84%	82.00%	93.80%

Conclusions and Discussions

The cortical thickness in the region pointed out in this paper play an important role in the classification. The mean and standard deviation of all vertices can construct effective discrimination algorithms. But the width of confidence intervals should be optimized. There is no confidences that could show one gold-standard criteria for separation.

The cortical thickness's measure methods can affect the exact values of thickness, but in many cases, including we proposed, the difference or the trends of cortical thickness across the whole brain are more useful. So our method does not have too much requirements for the exact measuring methods.

The limitation of this experiment is that the number of subject still arrives in a high quantity. And it is valuable to extend this experiment to more subjects.

Acknowledgements

This work was partially supported by Fundamental Research Funds for the Central Universities (No. JY10000904014) and Nation Scientific Foundation of China (No. 60802077 and 61003196). We really appreciate the Alzheimer's disease Neuroimaging Initiative (ADNI) (National Institutes of Health Grant U01 AG024904) and related contributions for the data share and collection.

References

- [1] Karama, S., et al., Cortical thickness correlates of specific cognitive performance accounted for by the general factor of intelligence in healthy children aged 6 to 18. *Neuroimage*, 2011.
- [2] Jubault, T., et al., Patterns of cortical thickness and surface area in early Parkinson's disease. *Neuroimage*, 2011. 55(2): p. 462-7.
- [3] Chen, Z.J., et al., Age-related alterations in the modular organization of structural cortical network by using cortical thickness from MRI. *Neuroimage*, 2011.
- [4] Fischl, B., et al., Automatically parcellating the human cerebral cortex. *Cereb Cortex*, 2004. 14(1): p. 11-22.
- [5] Worsley, K.J., et al., Detecting changes in nonisotropic images. *Human Brain Mapping*, 1999. 8(2-3): p. 98-101.
- [6] Westman, E., et al., Multivariate analysis of MRI data for Alzheimer's disease, mild cognitive impairment and healthy controls. *Neuroimage*, 2011. 54(2): p. 1178-87.
- [7] Zhang, D., et al., Multimodal classification of Alzheimer's disease and mild cognitive impairment. *Neuroimage*, 2011. 55(3): p. 856-867.
- [8] P. St-Jean, *et al.*, "Automated atlas integration and interactive three-dimensional visualization tools for planning and guidance in functional neurosurgery," *IEEE Trans Med Imaging*, vol. 17, pp. 672-80, Oct 1998.
- [9] C. Hinrichs, et al., "Predictive markers for AD in a multi-modality framework: an analysis of MCI progression in the ADNI population," *Neuroimage*, vol. 55, pp. 574-89, Mar 15 2011.

Dynamic analysis of an SIRS model with nonlinear incidence rate

Junhong Li^{1,a}, Ning Cui^{2,a}, Liang Cui^{3,b}, Caijuan Li^{4,a}

^aDepartment of Mathematics and Sciences, Hebei Institute of Architecture & Civil Engineering,
 Zhangjiakou Hebei, 075000, China

^acnmath80@163.com

^bOffice of Student, Shijiazhuang Tiedao University, Shijiazhuang Hebei, 051000, China

Keywords: SIRS model; global stability; Hopf bifurcation; limit cycle; simulation

Abstract. In this paper, we study the global dynamics of an SIRS epidemic model with nonlinear incidence rate. By means of Dulac function and Poincaré-Bendixson Theorem, we proved the global asymptotically stable results of the disease-free equilibrium. It is then obtained the model undergoes Hopf bifurcation and existence of one limit cycle. Some numerical simulations are given to illustrate the analytical results.

Introduction

Epidemiological models with variable population size have been studied by a number of authors [1-3]. Yu Jin et al [4] considered the global dynamics and bifurcation of an SIRS epidemic model with a nonlinear incidence rate. Liu et al. [5] introduced a nonlinear incidence rate of the form

$$f(I)S = \beta I^p S / (1 + \alpha I^q).$$

The global dynamics of an SIRS model with $p = q = 2$ and $p = 1, q = 2$ was studied [6-8], respectively. We assume the population can be partitioned into three compartments: susceptible, infectious, and recovered, with size denoted by S, I, R and susceptible and infective individuals have constant immigration rates. Based on [5-8], we construct an SIRS model that susceptible and infectious individuals have constant immigration rates. Namely, we consider the following SIRS model:

$$\begin{cases} S' = (1-p)B - \frac{\beta I^2 S}{1 + \alpha I^2} - dS + \varepsilon R, \\ R' = \gamma I - (d + \varepsilon)R, \\ I' = pB + \frac{\beta I^2 S}{1 + \alpha I^2} - (d + \gamma)I, \end{cases} \quad (1)$$

where the positive parameter d is the rate of natural death. ε is the rate at which recovered individuals lose immunity and return to susceptible class, γ is the rate for recovery. $(1-p)B, pB$ are constant recruitment of susceptibles, infectious, respectively. It is assumed that all the parameters are positive constants.

Thus the total population size N implies $N' = B - dN$. Since $N(t)$ tends to a constant as t tends to infinity, we assume that the population is in equilibrium and investigate the behavior of system on the plane $S + I + R = N_0 > 0$. So (1) becomes

$$\begin{cases} I' = pB + \frac{\beta I^2 (N_0 - I - R)}{1 + \alpha I^2} - (d + \gamma)I, \\ R' = \gamma I - (d + \varepsilon)R, \end{cases} \quad (2)$$

Qualitative analysis

In this section, we first consider the equilibria of system (2) and their global stability. Then we study the Hopf bifurcation and limit cycle. In order to find endemic equilibria of (2), we substitute $R = \gamma I / (d + \varepsilon)$ into $pB + \beta I^2 (N_0 - I - R) / (1 + \alpha I^2) = (d + \gamma)I$ to obtain the quadratic equation

$$f(I) = \left(\frac{\beta(d + \varepsilon + \gamma)}{d + \varepsilon} + d\alpha + \gamma\alpha \right) I^3 - (\beta N_0 + pB\alpha) I^2 + (d + \gamma)I - pB = 0.$$

From biological considerations, it is easy to see that $pB / (d + r) \leq I \leq N_0$, Direct calculations shows that

$$f\left(\frac{pB}{d+r}\right) = \frac{\beta N_0 p^2 B^2 [(p-1)(d^2 + d\gamma + d\varepsilon) - \varepsilon\gamma]}{(d + \varepsilon)(d + \gamma)^3} \leq 0,$$

$$f(N_0) = (1-p)B + \gamma N_0 + N_0^2 [\beta\gamma N_0 / (d + \varepsilon) + \gamma\alpha N_0 + (1-p)d\alpha N_0] \geq 0,$$

So we can easily see that system (2) has at least one endemic equilibrium $E_*(I_*, R_*)$. Let us now consider the stability of the endemic equilibrium. The Jacobian matrix of (2) at E_* is

$$J(E_*) = \begin{bmatrix} \beta I_*(1 - 2\alpha I_*^2)(N_0 - I_* - R_*) - \beta I_*^2 - pB / I_* & -\beta I_*^2 / (1 + \alpha I_*^2) \\ \gamma & -d - \varepsilon \end{bmatrix}$$

Let $R_0 = 2\beta / (\alpha pd)$. It is easy to obtain $tr(J(E_*)) < 0$, and $\det(J(E_*)) > 0$ when $R_0 \leq 1$.

The above discussin can be stated through a theorem.

Theorem1 The endemic equilibrium E_* of system (2) is locally asymptotically stable if $R_0 \leq 1$.

Theorem2 When $\varepsilon > \gamma$, the endemic equilibrium E_* of system (2) is globally asymptotically stable if $R_0 \leq 1$.

Proof. Taking Dulac function $D = 3N_0^2(1 + \alpha I^2) / (I^2\alpha(2d + \gamma + \varepsilon))$, we obtain

$$\begin{aligned} \frac{\partial(PD)}{\partial I} + \frac{\partial(QD)}{\partial R} &= -\frac{\alpha(2d + \gamma + \varepsilon)}{3N_0^2} I(3I + R) - \frac{6N_0^2 pB}{I^3 \alpha(2d + \gamma + \varepsilon)} - [\alpha(2d + \gamma + \varepsilon) - \\ &\quad \frac{2\alpha(2d + \gamma + \varepsilon)I}{3N_0}] - \frac{3N_0^2(\varepsilon - \gamma)}{\alpha(2d + \gamma + \varepsilon)I^2} < 0. \end{aligned}$$

Where (P, Q) is the vector field of (2). Obviously, $\partial(PD) / \partial I + \partial(QD) / \partial R < 0$ if $\varepsilon > \gamma$. Then by the Dulac's criteria, (2) admits no limit cycles or separatrix cycles. The global stability of E_* follows from the Poincare-Bendixson Theorem. This complete the proof.

In the following, we study the hopf bifurcation of system (2). For simplicity of computation, we consider the following system which is equivalent to (2)

$$\begin{cases} I' = pB(1 + \alpha I^2) + \beta I^2(N_0 - I - R) - (d + \gamma)I(1 + \alpha I^2), \\ R' = [\gamma I - (d + \varepsilon)R](1 + \alpha I^2), \end{cases} \quad (3)$$

Let $x = I - I_*$, $y = R - R_*$ to translate E_* to $(0, 0)$. Then (3) becomes

$$\begin{cases} x' = a_{11}x + a_{12}y + f_1(x, y), \\ y' = a_{21}x + a_{22}y + f_2(x, y), \end{cases} \quad (4)$$

Where $f_1(x, y)$ and $f_2(x, y)$ represent the higher order terms and

$$a_{11} = -2pB / I_* - \beta I_*^2 + (d + \gamma)(1 - \alpha I_*^2), \quad a_{12} = \beta I_*^2, \quad a_{21} = \gamma(1 + \alpha I_*^2), \quad a_{22} = -(d + \varepsilon)(1 + \alpha I_*^2).$$

To obtain the Hopf bifurcation, we fix parameters such that $tr(J(E_*)) = 0$, which is equivalent to $a_{11} = (d + \varepsilon)(1 + \alpha I_*^2)$.

Let $X = x, Y = a_{11}x + a_{12}y$. Then (4) is reduced to

$$\begin{cases} X' = Y + f_1(X, \frac{Y - a_{11}X}{a_{12}}), \\ Y' = -kX + a_{11}f_1(X, \frac{Y - a_{11}X}{a_{12}}) + a_{12}f_2(X, \frac{Y - a_{11}X}{a_{12}}) \end{cases} \quad (5)$$

Where $k = (1 + \alpha I_*^2)[\beta\gamma I_*^2 - (d + \varepsilon)^2(1 + \alpha I_*^2)] > 0$ if $I_* > \frac{pB\gamma + N_0(d + \varepsilon)^2}{\gamma(d + \gamma) + (d + \varepsilon)^2}$

Let $u = -X, v = Y / \sqrt{k}$. We obtain the normal form the Hopf bifurcation

$$\begin{cases} u' = -\sqrt{k}v + F_1(u, v), \\ v' = \sqrt{k}u + F_2(u, v) \end{cases} \quad (6)$$

Where

$$\begin{aligned} F_1(u, v) &= (d + \varepsilon)(1 + \alpha I_*^2)u^3 / I_*^2 + [\sqrt{k} / I_*^2 - 2(d + \varepsilon)(1 + \alpha I_*^2) / I_* + pB\alpha - 3d - 3\gamma + \\ &\quad \beta(N_0 - 3I_* - R_*)]u^2 + 2\sqrt{k}(1 + \alpha I_*^2)u / I_*, \\ F_2(u, v) &= -2uv(d + \varepsilon)\alpha(1 + \alpha I_*^2)\sqrt{k} / (\beta I_*^2)[\alpha(d + \varepsilon)^2(1 + \alpha I_*^2) / (\beta I_*^2) - \gamma\alpha]u^3 + \\ &\quad [\alpha(d + \varepsilon)(1 + \alpha I_*^2)(2d + 2\varepsilon + \sqrt{k}v / (\beta I_*^2) + 2\alpha\gamma I_*)u^2 + (d + \varepsilon)(1 + \alpha I_*^2)^2\sqrt{k}v / (\beta I_*^2)]. \end{aligned}$$

So we have the following Hopf bifurcation results

Theorem 3 There exist Hopf bifurcation and limit cycle in the system (3), when

$$a_{11} = (d + \varepsilon)(1 + \alpha I_*^2), I_* > \frac{pB\gamma + N_0(d + \varepsilon)^2}{\gamma(d + \gamma) + (d + \varepsilon)^2}. \quad (7)$$

To illustrate the results obtained, let us consider the following parameters $\alpha = 0.5$, and $B = 1, \gamma = 0.15, \varepsilon = 0.1, d = 0.2$ ^[7]. Then (7) holds. Thus, there is an limit cycle when $p = 0.001$ (see Fig 1-3) or $p = 0.01$ (see Fig 4)

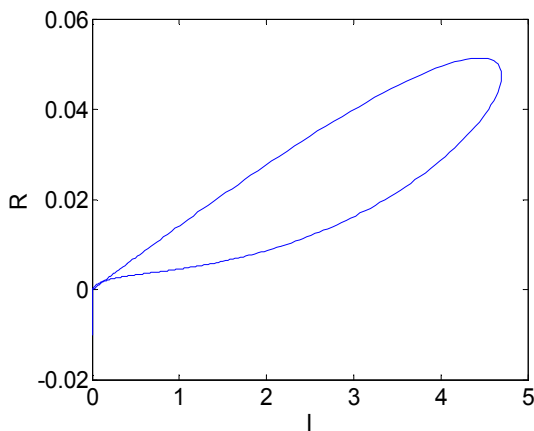


Fig.1. Limit cycle of (3) when $p = 0.001$

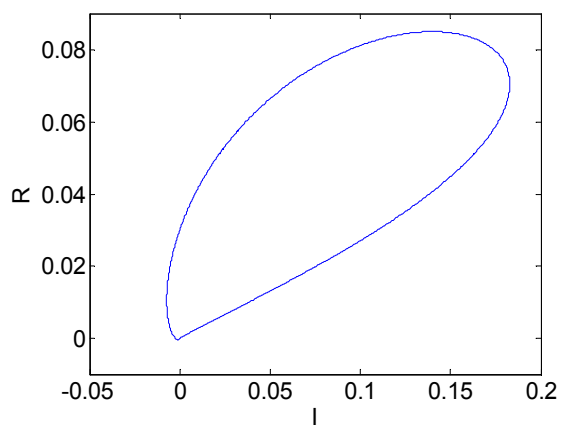
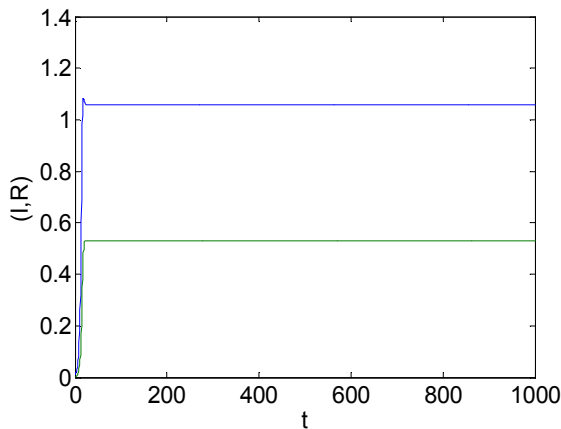
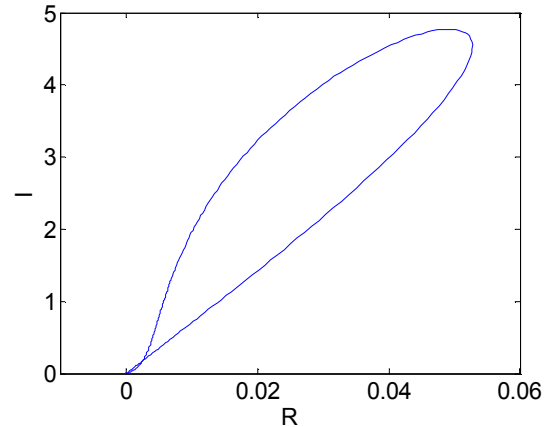


Fig.2. Limit cycle of (4) when $p = 0.001$

Fig.3. Time series of (3) with $p = 0.001$ Fig.4. Limit cycle of (3) when $p = 0.01$

Conclusion

In this paper we discuss an SIRS epidemic model with nonlinear incidence rate. We investigate the global dynamics of the reduced proportional system. And study the Hopf bifurcation and limit cycle of system (3). Without the recruitment of infectious, (1) becomes the SIRS model (see [6]). Finally, some numerical simulations are given to illustrate the analytical results.

Acknowledgement

Research is supported by the Youth Science Foundations of Education Department of Hebei Province : 2010233 and 2011236.

References

- [1] Zhixing Hu, Ping Bi, et al. Bifurcations of an SIRS epidemic model with nonlinear incidence rate. *Discrete and Continuous Dynamical Systems Series B*, 2011,15(1) 93-112.
- [2] Wendi Wang, Shigui Ruan. Bifurcations in an epidemic model with constant removal rate of the infectives. *J. Math. Appl.* 291(2004) 775-793.
- [3] G. Li, W. Wang. Bifurcation analysis of an epidemic model with nonlinear incidence rate. *Appl. Math. Comput.*, 214(2009) 411-423.
- [4] Yu Jin, Wendi Wang, Shiwu Xiao. An SIRS model with a nonlinear incidence rate. *Chaos, Solitons and Fractals*, 34(2007) 1482-1497.
- [5] W. M. Liu, S. A. Levin, Y. Iwasa. Influence of nonlinear incidence rates upon the behavior of SIRS epidemiological models, *J. Math. Biol.*, 23(1986) 187-204.
- [6] Ruan S, Wang W. Dynamical behavior of an epidemic model with a nonlinear incidence rate. *Journal of Differential Equations*, 188(2003) 135-163.
- [7] Dongmei Xiao, Shigui Ruan. Global analysis of an epidemic model with nonmonotone incidence rate. *Mathematical Biosciences*, 208(2007) 419-429.
- [8] T.K.Kar et al. Modeling and analysis of an epidemic model with non-monotonic incidence rate under treatment. *Journal of Mathematics Research*, 2010, 2(1) 103-115.

The design and development of a mass balance calculation software for sodium-calcium dual-alkali scrubbing flue gas desulfurization

Wenhui Pan ^{1,a}, Yixin Shi ^{1,b} and Jipu Liu ^{1,c}

Department of chemical process equipment engineering, Xiangtan University, Xiangtan 411105, People's Republic of China.

^a65849904@qq.com, ^bw7700928@126.com, ^cliujipu@yahoo.com.cn

Keywords: sodium-calcium dual-alkali method; desulfurization; mass balance; development of software.

Abstract. Based on the absorption principle of desulfurization process by sodium-calcium dual-alkali scrubbing method, the paper researches the computational model of gas balance, seriflux balance, and the circulating amount of seriflux, defines the equivalent relation between the data input and output, and develops a mass balance calculation software by Visual Basic 6.0. The software can be used for designing and equipment-selecting by employing the outcome of the computation. It can also do optimization and analysis of operation parameter. From the economic point of view, it is convenient for designers to choose the optimization parameter.

Introduction

According to statistics, there are over 200 kinds of methods of flue gas desulfurization technology at present around the world. Limestone/lime FGD is the most widely used, but it causes block and scale formation easily, and produces by-products of little use.

Sodium-calcium dual-alkali method is raised against the shortcomings of limestone method. Compared with limestone/lime method, Sodium-calcium dual-alkali method always uses the alkaline soluble supernatant to absorb, and pumps absorption solution out the absorption tower, then regenerates it with lime milk. Therefore, there is no block and scale formation. Through the regeneration reaction, the by-product can be use again, so that it is of much economic benefits.

The process system of Sodium-calcium dual-alkali scrubbing desulfurization

Process system. The sodium-calcium dual-alkali scrubbing desulfurization process system consists of flue gas system, desulfurizer circulation system in the tower and out the tower separately, by-products dewatering system, desulfurizer making system and other auxiliary system. The flow chart of Sodium-calcium dual-alkali FGD system is as shown in Fig.1.

After coming out of the dust remover of boiler, the flue gas will enter into desulfurization system form the lower part of absorption tower. When passing the pre-spray section, the flue gas will be cooled down abruptly, and then the flue gas will have a counter-current contact with sodium-calcium liquor sprayed from desulfurizer tower. Then multi-stage desulfurization reactions will happen, after this process, flue gas gets clean, then the clean flue gas needs to pass the demister device to demist and dewater, last, the gas will be discharged form the chimney. Absorbing liquid is pumped into spray pipe, and then will be sprayed down through the nozzle. The tower is decorated with 2-3 spraying layers so that the spraying liquid can cycle continuously, then the flue gas can be contacted and washed by the spraying liquid fully. The dust in the flue gas will be captured. The acid gas in the flue gas will finish the mass transfer and heat transfer chemical reaction with the absorption liquid on the surface of absorption liquid drop. Fresh absorption liquid enters into the system and the absorption liquid that already has reacted with flue gas and reached to a certain concentration will be pumped out the tower to regenerate.

Outside of the absorption tower, the absorption liquid that reached certain concentration is pumped into regeneration pool from the lower part of the tower to have the regenerating reaction with lime liquid. After the reaction, the seriflux will enter into the sedimentation pool, in where the solid and liquid will be separated; the clean liquid will enter into adjusting pool to complement sodium-calcium so that the clean liquid can reenter absorption tower to cycle. After depositing, the desulfurization slag is pumped to by-product dewatering system to dewater.

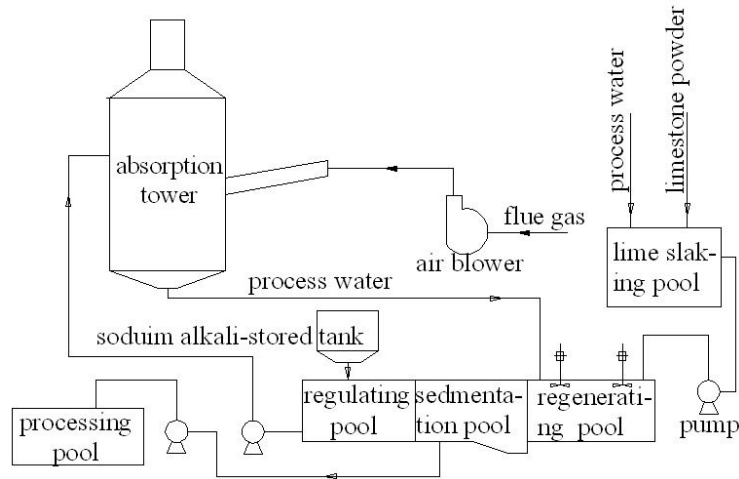


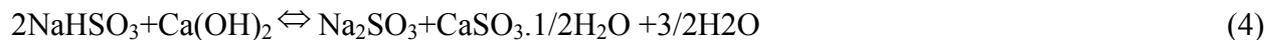
Fig.1. The flow chart of Sodium-calcium dual-alkali FGD system

Absorption principle

Desulfurization reaction



Regeneration reaction



Oxidation reaction (side reaction)



Model of calculation

In the whole system flow, on the basis of material balance in the absorption tower, the material amount of each input devises and output devises can be calculated. According to the law of conservation of mass, the input material mass of system = the output material mass of system + accumulated material mass in the system.

Material balance in the absorption tower. The principle of sodium-calcium dual-alkali method is making the sodium alkali contacted with flue gas that containing SO₂, then chemical reaction will happen so that SO₂ will be removed. In the absorption process, the absorbent in which mainly sodium alkali is working is on the basis of solution mixture, and the fresh desulfurization liquid is inputting continually. The desulfurization liquid after fully reacted with flue gas will flow out of the tower and then get into the regenerating cycle outside of the tower.

The input material of absorption tower system includes 5 parts, they are sodium alkali solution, flue gas, process water, water for cleaning and oxidation air. Output material is consist of two parts, clean flue gas and sodium alkali desulfurization liquid at certain concentration.

In fact, there are several complicated side reactions in the calculation, but for the reason that sodium is used only in the cycling system out of the desulfurization tower and the loss of sodium only exists in the water that drained off and desulfurization slag in the cycling process, so it affects the calculation a little and can be ignored.

The material balance of regenerating system. The desulfurization liquid that flow out of tower will go into regenerating pool first, then will have replacement reactions with lime liquid, and last will go into sedimentation tank to precipitate. The sediments will be divided into 2 parts. One part is upper liquids that will go to water pool and then reenter absorption tower on the work of cycling pump, the other part is desulfurization slag that contains about 20% water. Because there will be loss of hydroxide sodium in the desulfurization slag, so hydroxide sodium should be complemented periodically.

The balance of water. The process water that enters into FGD system contains sprayer clean water, water contained in sodium alkali complement, pump and tube clean water, lime solution water, vacuum pump sealing water and buffer pool complement water. The water that flows out of system contains plaster crystal water, water contained in desulfurization slag, evaporation water of absorption tower and water contained in drained off filter liquor.

The amount of cycling liquid. In the desulfurization chemical reaction process, there always exists chemical absorption. So, the amount of cycling liquid we should considered the chemical absorption.

Designing of software for calculating material balance

Based on the calculation model above and visual basic 6.0 designing platform, Excel VBA language is used as the tool to design the software that uses sequential modular approach to simulate the process. Each dual-alkali flue gas desulfurization step will be seen as a unit, and then a program will be written for each unit. In the program, output material variable will be regarded as the function of input material variable and devices parameter. This calculation software adopts the ADO subject to visit the database of SQL SEVER, in which, there keeps a lot of application data of the software. While calculating, it is very convenient to read data, save data and export results (in excel table form) to use the software.

The interface of software. The interface of the software is shown in Fig.2. The interface element consists of environmental data, the parameters of the inlet flue gas of the FGD system, the concentration of other pollutants, the equipment parameters of the absorption tower and the boiler parameters and so on. For specific Sodium-calcium dual-alkali scrubbing desulfurization projects, user only need to input the system configuration and the initial parameters, then click the calculation button, we can do the mass balance calculation work. At the same time, using the data output menu bar option of the software, the calculation can be exported in the form of Excel files. The files consist of the calculation table of the gas balance, the seriflux balance, and the mount of seriflux.

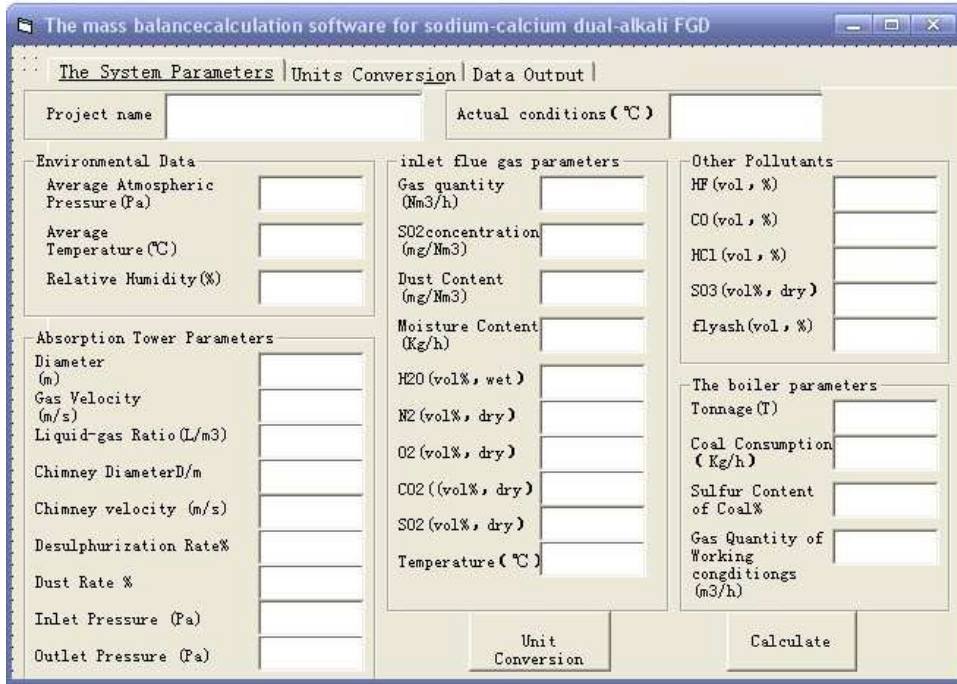


Fig.2. The main interface of calculation software

The example of the application of software in the engineering. Taking the sodium-calcium dual-alkali FGD system of an electric power company as an example. The boiler is 35T, the flue gas quantity is 75673.5542Nm³/h, and desulphurization rate can reach 96%. We input the parameters in the software interface as shown in Fig.2, click the calculation button, after calculating, we can get the data consists of the gas balance chart of dual-alkali FGD system as shown in Fig.3, the seriflux balance chart of dual-alkali FGD system as shown in Fig.4, and the amount of seriflux as shown in Fig.5.

Name	Molecular Weight (kg/mol)	Volume Fraction (%)	Exhaust Fan Entrance / (kg/h)	Spray Entrance of Tower/ (kg/h)	Spray Outlet of Tower/ (kg/h)	Tower Entrance / (kg/h)	Tower Outlet / (kg/h)	Atmosphere / (kg/h)
N ₂	28	73.5000	69525.0779	69525.0779	69525.0779	69525.0779	69525.0779	69525.0779
CO ₂	44	13.8000	20512.9384	20512.9384	20512.9384	20512.9384	20512.9384	20512.9384
O ₂	32	5.0000	5405.2539	5405.2539	5405.2539	5405.2539	5405.2539	5405.2539
SO ₂	64.06	0.0862	186.4800	186.4800	186.4800	186.4800	7.4592	7.4592
SO ₃	80.06	0.0004	0.9842	0.9842	0.9842	0.9842	0.6889	0.6889
HCl	36.5	0.0005	0.6151	0.6151	0.6151	0.6151	0.0123	0.0123
HF	19.998	0.0005	0.3691	0.3691	0.3691	0.3691	0.0111	0.0111
CO	28	0.9200	870.2459	870.2459	870.2459	870.2459	870.2459	870.2459
H ₂ O	18	6.7500	4104.6147	4104.6147	7768.1119	7768.1119	10358.0787	10358.0787
Flyash	-	0.0000	8.4000	8.4000	8.4000	8.4000	2.9400	2.9400
TOTAL		100.0576	100614.9792	100614.9792	104278.4764	104278.4764	106682.7064	106682.7064

Fig.3. The gas balance chart of dual-alkali FGD system

NAME	Molecular Weight	Ca(OH) ₂ Warehouse	Na ₂ CO ₃ Warehouse	Absorption Liquor from Circulating Pump	Seriflux export from tower	After Regeneration	After Precipitation	Regulating Pond	Water Supply for Demister
Na ₂ SO ₃	126.04	0	0	306.44	0	352.23	352.23	352.23	
NaHSO ₃	104.16	0	0	0	582.17	0.00	0.00	0.00	
Gypsum	172.14	0	0	0.00	0.00	481.06	0.00	0.00	0.00
Ca(OH) ₂	74.09	207.05	0	0.00	0.00	0.00	0.00	0.00	0.00
Na ₂ CO ₃	105.99	0	38.51	38.51	0.00	0.00	0.00	38.51	0.00
Fly ash		0	0	0.00	5.46	5.46	0.00	0.00	0.00
Water	18	0	0	252686.60	252636.30	252686.60	252686.60	252686.60	50.30
Total		228.13	38.29	253032.08	253225.72	253544.52	253038.83	253077.87	50.30
Flow m ³ /h				240.94	238.89	236.96	240.99	241.03	0.05
Relative Density		2.24	0.90	1.050	1.060	1.070	1.050	1.050	1.000
Temperature °C		25.00	25.00	55.00	55.00	55.00	55.00	55.00	25.00
PH				7-8	5-6	7-8	7-8	7-8	6~7

Fig.4. The seriflux balance chart of dual-alkali FGD system

SO ₂ Ew in the water of 55°C	9.91E+03 Kpa				
Na ₂ SO ₃ :h ₁ =	-0.003 m ³ /Kmol	I ₁ =	0.030272994 Km ³ /m ³		
Na ₂ CO ₃ :h ₂ =	0.0449 m ³ /Kmol	I ₂ =	0.004523551 Km ³ /m ³		
lg(E/Ew)=	0.0001123	E=	9907.561306Kpa	m=	92.313639
SO ₂ Concentration of Inlet tower			1739mg/m ³		
Equilibrium Temperature in tower			55°C		
Gas Concentration of Inlet Tower		Y ₁ =	0.000812282 Km ³ SO ₂ /Kmol gas		
Gas Concentration of outlet Tower		Y ₂ =	3.24913E-05 Km ³ SO ₂ /Kmol gas		
Liquid of Inlet Tower		X ₂ =	0		
(L/G) min=	(Y ₁ -Y ₂) / (Y ₁ /m-X ₂)=	88.62109344 Km ³ Absorption liquid/Kmol gas			
The amount of cycling liquid	L=	(L/G) min*G	=	349356.1 Km ³ /h	
		=	74.571201L/Nm ³	=	6288409 Kg/h = 5989 m ³ /h
Considered the desulphurization rate is 96%			L=	6199 m ³ /h	

Fig.5. The amount of cycling seriflux

Conclusion

This paper considers the principle of dual-alkali method desulfurization process as the starting point, analyses the material balance model of dual-alkali method desulfurization process, and furthermore designs a kind of software to calculate the material balance in the dual-alkali method desulfurization process in EXCEL using the Visual Basic 6.0 software. This calculation results are reliable and it is ease to operate. The data exported by this software can be used as technical data for operation parameter optimization, system debugging, and economical efficiency improving.

References

- [1] MARK A. SGAND. A New Look at SO₂ Removal. Pulp& Paper International 2009, 51(4).
- [2] D.L.Jian, Q.G.Zhou. Current status and expectation on desulfurization of the thermal power plant [J]. Energy environmental protection, 2006, 20(3): 48-51.
- [3] Z.B.WU, Y.Liu and T.E.Tan. Study of dual-alkali FGD process [J]. Acta Scientiae Circumstantiae, 2001,21(05): 534-537.
- [4] F.Lu; S.M.Liu; Y.C.Zheng; B.Zou. Technology of Na-Ca Double Base Process of Flue Gas Desulfurizing[J]. Guangdong Chemical Industry, 2010 37(203): 159-160.
- [5] From Accidence to Mastery for Visual Basic 6.0. Beijing: Electronic Industry Press,2008.

Numerical Simulation of 2-D Two-phase Flow Field Covered by Vegetation Dam based on Fluent Software

Feng Liu^{1,a}, Liang Ma^{2,b}, Liang-liang Chen^{2,c}, Guang-hui Wei^{2,d}

¹Division of Development and Programming, Xinjiang Agricultural University, Urumqi, China

²School of Water Resources and Civil Engineering, Xinjiang Agricultural University, Urumqi, China

^awlmqlf1999@163.com, ^bxjml1999@163.com, ^cxndc11@163.com, ^dxndwgh@163.com

Keywords: vegetation dam; Fluent; numerical simulation

Abstract.In this paper, the hydrodynamic equation about the flow through plants has established through the physical model experiment and theory deduction, the hydraulic characteristics of vegetation dam has simulated with the established equation. The two-phase flow field of the water sink with plant dam overlay has simulated with software of FLUENT, and the free surface has been tracked with VOF method, the plant dam overlay districts has been simplified with many bores area method, and the infiltration rate has been determined with the pressure difference of before or after bores area. The simulation velocity magnitude is compared well with the measured data.

Introduction

In 1995, professor Bi Ci-fen, Li Gui-fen and Yu Zhuo-de pointed out that: Soft rock channel runoff capacity of soil erosion on coarse, torrential rain and flood erosion characteristics of a single main proposed the use of sea buckthorn plant "flexible dam" to intercept gully grit. After several years, which have been part of the coarse solid in the gully, reducing the grit into the Yellow River, but also to the ecological environment in these areas to improve. The so-called sea buckthorn plant "flexible dam" (referred to as plant dam) is the main canals in the channel or tank, at a certain spacing and line spacing, planting a number of sea buckthorn plants. After investigation, soft rock are also common in Xinjiang, and its living environment even worse, resulting in relatively more coarse, so the more urgent need to address. Plants for the western region of the dam, especially in the sand for the Xinjiang region, combating desertification and soil erosion has provided a new ideas. Institute of Water Resources and Hydraulic Engineering Laboratory, Xinjiang Agricultural University, in 2002 and 2003, studies indoor plant dam water tank model tests, which examine the plants in the ranks of the aligned and staggered dam layout, different planting density on the canals the impact of water[1,2]. To further study the water plant mechanical properties over the dam and fixing mechanism, the group muddy water tank for the indoor use of Fluent software model test and coverage of plant dam the flow field was simulated.

Establishment of the basic equation

Generating plants in canals behind the dam, the water is still available plant leaves incompressible viscous fluid of the basic equation—NS equations to describe. If the canals in the category of sea buckthorn shrub vegetation, although this time the vegetation can still be handled as a water boundary, but the vegetation itself is extremely complex boundary shape in the water will be produced in the bending deformation, and in its equilibrium position to do small vibration, which makes the boundary conditions and an overview of the more complex elements of the subdivision. Therefore, the establishment of trees flow mathematical model of the most crucial question is how to deal with flexible vegetation boundary. For this problem, consider the trunk in the water occupies the volume ratio, the plant dam extended to long enough to plant groups[3], and based on mass conservation and Newton's mechanics, assuming infinitesimal hexahedron, try to derive trees water the basic equations, including continuous equation and the equation of motion is given by:

Continuity equation:

$$(1-\eta_x)\frac{\partial(\rho u)}{\partial x}+(1-\eta_y)\frac{\partial(\rho v)}{\partial y}+(1-\eta_z)\frac{\partial(\rho w)}{\partial z}-\rho u\frac{\partial\eta_x}{\partial x}-\rho v\frac{\partial\eta_y}{\partial y}-\rho w\frac{\partial\eta_z}{\partial z}+\frac{\partial}{\partial t}[\rho(1-f_v)]=0 \quad (1)$$

Equations of motion:

$$(1-\eta_x)\frac{\partial p_{xx}}{\partial x}+(1-\eta_y)\frac{\partial \tau_{yx}}{\partial y}+(1-\eta_z)\frac{\partial \tau_{zx}}{\partial z}-\left(p_{xx}\frac{\partial\eta_x}{\partial x}+\tau_{yx}\frac{\partial\eta_y}{\partial y}+\tau_{zx}\frac{\partial\eta_z}{\partial z}\right)+\rho X(1-f_v)-f_{Rx}=\rho(1-f_v)\frac{du}{dt} \quad (2)$$

The equation (1), (2) are the basic equation of water trees can be seen, the role of vegetation makes the equation because the unknown is greatly increased. When the canals are no trees, then the above formula can be simplified as:

$$\begin{cases} \frac{\partial(\rho u)}{\partial x}+\frac{\partial(\rho v)}{\partial y}+\frac{\partial(\rho w)}{\partial z}=\frac{\partial\rho}{\partial t} \\ \frac{\partial(\rho u)}{\partial t}+\frac{\partial(\rho u^2)}{\partial x}+\frac{\partial(\rho uv)}{\partial y}+\frac{\partial(\rho uw)}{\partial z}=\rho X+\frac{\partial p_{xx}}{\partial x}+\frac{\partial \tau_{yx}}{\partial y}+\frac{\partial \tau_{zx}}{\partial z} \end{cases} \quad (3)$$

Numerical simulation

Water flow within the plant dam can be seen as a porous media flow[4]. Whether physically or mathematically, the pores within the porous media flow is a very complex flow phenomena, this paper make the following assumptions:

The porous medium is isotropic, homogeneous rigid media;

The upper boundary of the rigid porous permeable boundary.

Porous media model assumptions and limitations

Porous media model uses the empirical formula defines the flow resistance of porous media. In essence, the porous medium model is an increase in the momentum equation in the consumption of a representative momentum source term. Therefore, the porous medium model needs to satisfy the following constraints:

Because the volume of porous media is not reflected in the model, by default, FLUENT in porous media using the name based on the volume flow rate to ensure that the velocity vector in the continuity through porous media. If you want more precise calculations, but also allows FLUENT in porous media using real speed;

Effects of turbulence in porous media is only approximate;

Coordinate system used in the mobile model porous media, you should use the relative coordinate system, rather than the absolute coordinate system, in order to guarantee the correct source term solution.

Treatment of porous media model to turbulence

FLUENT calculated in porous media by solving the standard conservation equation turbulence model variables[5]. In the calculation process, usually assuming the solid medium on the generation and dissipation of turbulence has no effect. Great permeability in porous media, thus the medium-scale geometric structure of the turbulent eddies have no effect, this assumption is reasonable. In some cases, may need to consider the turbulent flow, assuming that flow is laminar. If the turbulence model used in the calculations is the k-ε, k-ω or Spalart-Allmaras model in one, the turbulent viscosity μ can be set to zero in approach ignores the impact of turbulence[6]. If the turbulent viscosity μ is set to zero, then the calculation will still transport the variable turbulence the other side of the media, but the process of turbulent transport of momentum effect is completely eliminated. In the area of fluid panel will set the layer porous media flow area option can be set to zero turbulent viscosity μ.

Finite thickness of the porous media is Darcy's law the pressure change and an additional inertial loss term defined.

Meshing

Meshing is an important branch of computational fluid dynamics, using a discrete numerical grid instead of the original physical problem in continuous space, the grid nodes is solved by the geometry of physical quantities[7], need to calculate the area of the mesh, and then in the division on the grid discrete equations, solution.

In this paper, the more commonly used GAMBIT mesh generation software, choose the model structure of the grid mesh partition, so to ensure the quality of the grid, reducing the overall number of grid cells, while a good test to verify the physical a cross-section measurement results for the object. Plant cover section of the dam to generate grid cell of about 2800, about 2911 mesh nodes. Grid cells in other regions around 4641, mesh nodes about 7200.

Setting the boundary conditions

In the numerical simulation of the flow domain is driven by the boundary conditions[8], in a sense, the process of solving practical problems is the boundary line or boundary surface of the data, extrapolated according to equation extended to the computational domain internal process. Therefore, the provision in line with the physical reality and the appropriate boundary conditions is extremely important. Set boundary conditions must be guaranteed in the right place to choose the right boundary conditions, while allowing the boundary conditions do not over-constrained, and do not owe constraints. This water-gas two-phase flow field calculations for which the boundary conditions are: import boundary conditions, the outlet boundary conditions, the solid wall boundary conditions and free surface.

Numerical calculation

This numerical model of the process in two steps, first simulated tank covered when the dam is no plant water flow steady stream, until convergence, and convergence in the simulation based on the flow field within the tank when the water plant dam covered the unsteady two-phase gas stream flow. Otherwise, if the direct simulation of gas-water two-phase unsteady flow, iterative calculation is easy to divergence[9]. On this basis, then the application of VOF method to capture free water into water vapor two-phase unsteady flow simulation. Numerical model of the flow inlet boundary conditions are used to set the speed entrance, when the water inlet of the actual water level under the experimental conditions set; the entrance to the downstream of the cross section above the water level is set to import gas pressure, static pressure is set to 0; downstream export into the air exports and exports of liquid water flow in two parts, the air pressure to export part is exported, static pressure is 0; the boundary conditions of the turbulence parameters are determined in accordance with empirical formula turbulent kinetic energy dissipation rate, solid side wall roughness equivalent to 0.05m to take test . Pressure interpolation format selected body force weighted format, momentum, turbulence energy, turbulence dissipation rate are first-order upwind discretization scheme. The time step 0.001 second, needs to set the time step 100000, within each time step the maximum number of iterations is 20.

Figure 1 shows the vertical velocity within the plant dam experimental and calculated values. It can be seen from the figure, the experimental values in agree well with the calculated values, indicating that the numerical model is more accurate.

At the same time, can also be seen in Figure 4,calculated flow rate by the value of the test than the test derived from the flow rate is greater. Not limited to a few points, but the overall test is greater than the calculated values. This phenomenon is mainly due to the numerical calculation, reduce or ignore some resistance factors, such as the bottom of the resistance, surface wind stress and so on. In the actual flow field, such resistance exists.

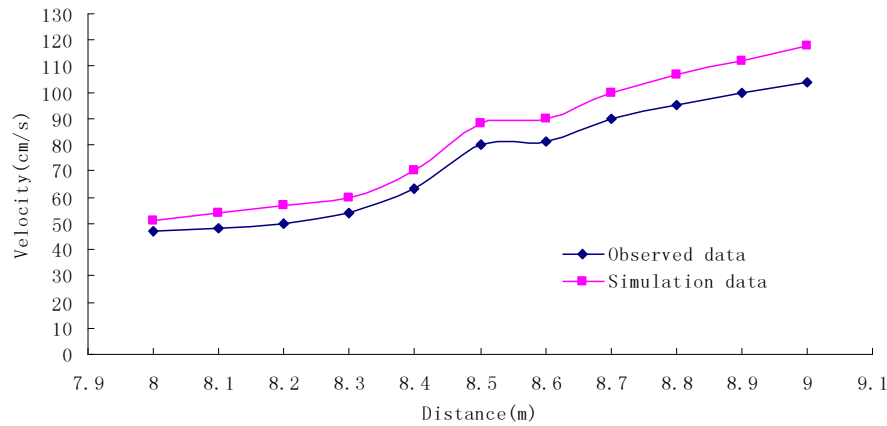
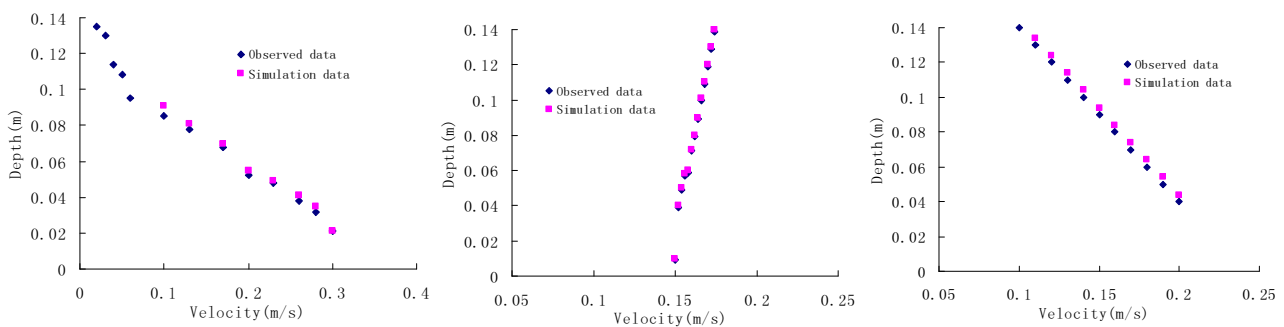


Fig.1. Comparison of dam vertical velocity testing and calculated values

Here is a plant dam simulate three typical cross-section tank cover (plant dam front, middle dam plants, plant dam at the end) on the velocity with the experimental value of the comparison figure.



a. Flow rate comparison in the front of plant dam

b. Flow rate comparison in the middle of plant dam

c. Flow rate comparison at the end of plant dam

Fig.2. Compared with the experimental values and simulation values

When water flow through the plant dam, with the dam blocking water produced by plants obstruct high flow velocity decreases rapidly; water flow to plant the middle of the dam, the flow rate stabilized, the flow rate value on the longitudinal section along the water depth changed little; water By the end of plant dam, the flow of water by plant foliage reaction effect increases with the depth of the flow rate value is again reduced.

In Figure 2, we can see that, the simulation of three sections on the velocity distribution along the depth trends and test the measured results are in agreement. It is suggested that this calculation using Fluent software and VOF method coupled mathematical model is correct, use of plant dam-domain simulation in porous media coverage is feasible.

Conclusions and discussion

Through experiment phenomena and numerical simulation results of the analysis, we draw the following conclusions:

After place the plant "flexible dam" in the sink, the flow field has been significantly different with before in the water tank, which is a plant dam upstream backwater area upstream flow blocking effect of the direct results.

Compare simulation value of velocity with measured value, both in good agreement. It show that the mathematical model is correct, use plant dam-domain simulation in porous media coverage is feasible.

The existence of plant "flexible dam" interference with the original flow pattern, the tank water before the flow field and tree planting has been significantly different. Each plant trees within the dam, is a very complicated boundary conditions the flow around the problem, in their joint action produces a row of trees blocking effect on the water, and thus the formation of the whole plant dam

effect, making the plants inside the tank dam tour section kinetic energy to overcome plant resistance generated by the dam on the flow, resulting in plant dam backwater tour, behind the dam erosion phenomenon. Backwater upstream of the dam in the plant area after planting the cross-section of the flow velocity is less than before planting, and the more the smaller the flow rate near the plant dam, can better explain the decrease of plant dam dam dam and the average flow rate, peak flow rate can be homogenized. Therefore, plants in the natural channel upstream of dam sediment can reduce the starting frequency, and make the start of the sediment has been deposited, so as to achieve sand, sediment effect. Flow rate calculated by the numerical model and physical model tests the value of the comparison value may indicate that use of Fluent software to calculate and VOF method coupled mathematical model is correct, use of plant dam-domain simulation in porous media coverage is feasible. In this paper, a more systematic experimental study of plant analysis of the river dam, has been a lot of valuable data and conclusions, so we have a plant dam the river flow characteristics with a further understanding of the problem, but only a preliminary study, also to be in-depth theoretical analysis and mathematical tools used more, do more physical model tests and numerical simulation studies.

Acknowledgement

This research work was supported by Xinjiang Agricultural University Pre-school Funding Project(XJAU201008). We give the most heartfelt thanks to the reviewers for their great contributions on the early manuscript.

References

- [1] Cheng Yan, Li Sen, Qiu Xiu-yun, etc. Study on flow characteristics of rivers and canals trees. *Journal of Xinjiang Agricultural University*,2003,26(2):59-64.
- [2] Yan Jie, Zhou Zhu, Qiu Xiu-yun.Plant flexible dam test and fixing water blocking mechanism analysis. *Journal of Xinjiang Agricultural University*,2004,27(3):40-45.
- [3] Shi Bing, Cao Shu-you.Plant Sand Dynamics.Qingdao: Qingdao Ocean University Press,2000.
- [4] Huai Wen-xin,Han Jie,Zeng Yu-hong.Velocity distribution of flow with submerged flexible vegetations based on mixing-length approach.*Applied Mathematics & Mechanics*,2009,(3):151-158.
- [5] Wang Fu-jun *Computational Fluid Dynamics analysis—CFD Software Principles and Applications*. Beijing: Tsinghua University Press,2004.
- [6] Zhang Ben-zhao. *Hydrodynamics numerical methods*.Beijing: Mechanical Industry Press,2003.
- [7] Zhang Ming-liang,Chen Yong-ming,Wu Xiu-guang,etc.Compound section three-dimensional numerical simulation of floodplain flow. *Journal of Hydroelectric Engineering*,2006,(5):16-19.
- [8] Huai Wen-Xin, Han Jie, Zeng Yuhong. Experimental study on hydraulic behaviors of steady uniform flow in open channel with submerged flexible vegetation.*Journal of Hydraulic Engineering*,2009,(7):34-40.
- [9] Huai Wen-xin,Xu Zhi-Gang,Yang Zhong-hua. Two dimensional analytical solution for partially vegetated compound channel flow. *Applied Mathematics & Mechanics*,2008,(8):135-139.

Efficient Data-Parallel Algorithm for Elevation Color Generation in Terrain Rendering

Zhengkang Zhou^{1, 2, a}, Jian Wang^{1, b} and Huacheng Zhao^{1, c}

¹ Department of Computer Science and Technology, Xi'an Jiaotong University, Xi'an 710049, China

² Department of Foundation, Xi'an Communication of Institute, Xi'an 710106, China

^azzkshaanxi@163.com, ^bwangjianjunan@163.com, ^cz151614650@126.com

Keywords: algorithm; elevation color generation; data parallel; CUDA; terrain rendering.

Abstract. With the ever increasing resolution of scanned elevations, the efficiency of terrain rendering is still unsatisfactory in three-dimensional visualization. In order to improve the speed of terrain rendering, we had studied the root cause of the undesirable visualization efficiency in Visual Terrain Project, and found that one of the performance limitations was elevation color generation step. Therefore, we proposed a modified algorithm on the basis of data parallel mode, which can be well performed on GPU. Experimental results show that application performance is raised significantly by data parallel algorithm, and the improved algorithm can obtain satisfactory simulation results via CUDA.

Introduction

Traditionally, in order to achieve more realistic terrain maps, researchers used to generate different color to different elevation gradually [1]. Virtual Terrain Project (VTP), based on OpenSceneGraph (OSG), aimed to foster the creation of tools for easily constructing any part of the real world in interactive, 3D digital form. The class library of VTP applied the elevation based color generation method to present different color to responding elevation [2].

Along with the ever increasing resolution of scanned elevations, we are too distraught to face the inefficient of terrain rendering. In the wake of the increasing of terrain size, the performance of system reduced by a wide margin especially the execution time. We tracked the source code to find out restrictions of our system. It was extremely urgent for us to figure out some effective ways to improve execution efficiency.

The rest of the document is organized as follows. In Section 2, there is a list for some related works. In Section 3, we provide a conditional operational process for elevation generation. A modified process based on data parallel mode is presented in Section 4, comparing the conditional one. In order to evaluate the new algorithm, experimental data and statistical results are put forward in Section 5. Other results are summarized and future works are outlined in the last Section.

Related Work

A number of previous efforts have tackled to describe terrain elevation. Mark Deloura mentions a Square-Diamond Algorithm in procedure generation [3]. And Andre LaMothe in his book presents us two different means in implementation, fractal terrain generation and procedure generation [4]. In order to enhance the sense of reality for terrains, people tended to take relief shading in their projects. In recent years, researchers brought elevation based color generation method into use, especially in the field of computer 3D visualization [5]. Meanwhile, with the development of level of details, grid method has been used more and more widely.

Due to the ever increasing size and resolution of scanned digital elevation models (DEMs) and corresponding photo textures, a lot of research works have been done to improve the process of terrain rendering. With the purpose of displaying massive terrains in real time, a number of researches focused on three major types of technique required for texture management and mapping: On the one hand, applying specific structures to organize a number of available texture (and geometry) sets,

DEM [6] and BT. On the other hand, inventing complex level-of-detail computation. Besides, finding effective methods to eliminate redundant data, like ray-casting [7]. Recently, with the purpose of accelerating the rendering process, part of the work has been transferred to GPU [8], which supports a parallel programming environment [9].

Conditional Elevation Based Color Generation Algorithm

Relevant Contents in VTP. VTP aimed to foster the creation of tools for easily constructing any part of the real world in interactive, 3D digital form. The class library of VTP applied the elevation based color generation method to present different color to responding elevation.

Detailed analyses of operations are as follows. Locate the running entry of our system so as to track the source code. In the process of creating terrain, VTP provide us a global variable named vtScene. First we initialized the environment and pass address parameters to object vtScene by function vtGetScene(). Then we created new object named vtTerrainScene, which was applied to generate three-dimensional terrain. At the same time we created a scene group and added vtScene to them. We ran the program to generate a three-dimensional terrain object, passed the configuration file to this object. In the following we had to render terrains by function BuildTerrain() after added the object to the terrain scene. Two of last works were adding flight engineering and mouse controlling.

Conditional Elevation Color Generation. The main idea of this conditional algorithm is that the same elevation should be rendered the same texture color. In fact, several principles need to be complied with this algorithm: First of all, the color for each level of the elevations should be changed gradually responds to the changing elevation. In addition, the color chart should be created according to the three-dimensional efficiency of color. Finally, choosing the specific color should meet appropriately geographical landscape color and people's visual habit [10]. For instance, usually, blue presents sea level as well as green equal to horizon.

Algorithm description of the elevation based color generation method:

Step1: First, loading the terrain XML file, then checking that whether the value of Color_Map is existed. If any, load the Color_Map attribute description file defalut_relative.cmt; else then generate the default Color_Map file.

Step2: Obtain height and width of the terrain meshes; besides, get the value of the both maximum and minimum elevation within the confine of elevation meshes.

Step3: Trying to corresponding elevation value which figured out by one-dimension linear interpolation to color table one for one. And then generate the color table for this algorithm.

Step4: While index terrain elevation value via line number; traverse the whole nodes of terrain meshes. Then convert elevation value indexed to color table subscript by linear interpolation.

Step5: End.

In the process of program execution, we figured out the execution time of each step in the algorithm above through adding in compiler timestamp. Our analysis of merely a hundred exponents indicates that the third and forth step is the most time-consuming. Take the terrain with 8193*8193 resolution for example, the exaction time of these two steps cost almost whole time of the algorithm when input this terrain mesh. This result was even proved while terrain's resolution increases. It is obviously that this two steps mainly to generate corresponding relation between e elevation and color.

Based on Data Parallel Elevation-Coloring Algorithm

In the context of modern 3D applications, CPU overhead is a common drawback. To overcome this limitation, we present a data parallel based elevation based color generation algorithm using CUDA (Compute Unified Device Architecture) in this paper. This modified solution was formed through analysis the main disadvantages of the original algorithm carefully. After the rewriting of the algorithm, the time-consuming parts were successfully transferred to GPU which would be carried out by data parallel mode [11].

The algorithm of elevation based color generation color-setting based on GPU acceleration was on the basis of former's improvement. The principles are to optimize the most time-consuming phase of the former algorithm for CUDA parallel processing and complex general calculating by GPU. We changed the name of the algorithm to BDPEC. In order to make the codes well suitable to run on GPU, firstly, we need to prepare the data which should be processed by GPU. Then with this prerequisite of not effecting algorithm functions, change the structure of the algorithm, replace the statements for the function call for statements of the non-function call to eliminate those statements which will affect the parallel performance. We can see from Step4 that is mainly loop and iterate through every node of the grids to achieve the elevation values. The flows of the improved algorithms are shown by Fig. 1.

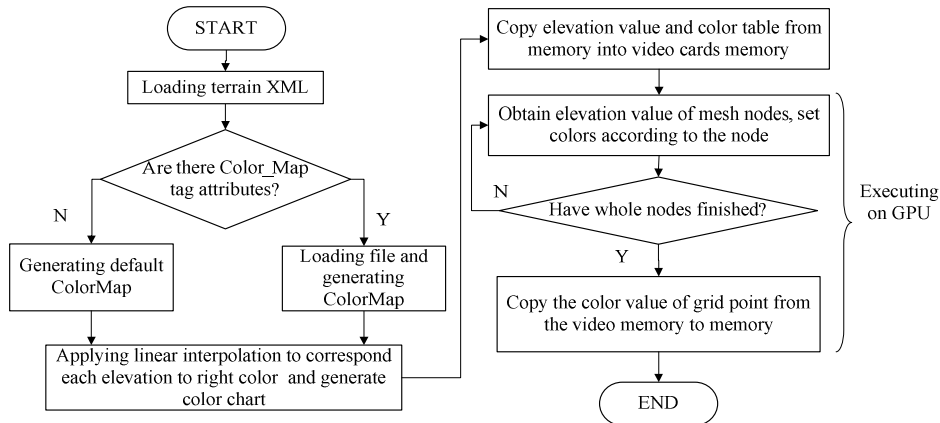


Fig.1. Algorithm Diagram

Improvement of Data Structure. When we utilize CUDA to program, we should prepare the data which calculated for the graphics card, and copy the data from CPU to GPU. Thus we need to place the elevation values of terrain grids in the arrays, which may directly copy the data involved in the calculation to GPU. The data structure of array goes especially well with data parallel by GPU, which may map the data in the array to every thread of parallel processing in parallel mechanisms.

After rewriting the data structure of the original algorithm as well as storing the data to deal with in the array, we finally copy the data into the graphics card by calling Memcpy() of CUDA API.

Complete Computation on GPU. There exist certain equivalence relations between the kernel functions Of GPU and the cycles on the CPU. GPU's multiple SM is its processor which performs calculations on datasets while CPU using an iterative method for sequence processing of datasets. SM can be applied to all elements of datasets by writing similar instructions in one kernel of GPU. Therefore the algorithm operating on GPU means accelerating based on data parallel mode.

Data and Results

In this section, we present a detailed analysis of the performance of both the original and the improved algorithm. All benchmarks were run on a standard desktop PC, equipped with a Pentium Daul E2160 1.8GHz processor CPU, 2.0GB of RAM, and an NVIDIA GeForce 9500GT graphics card with 128MB of global memory. The programs executed on such a software environment that Visual Studio.NET 2003, CUDA Toolkit1.1 and CUDA SDK1.1.

Data Sets. For our tests, we used five group datasets of different resolution ratio. All these data sets are digital model of the middle and lower reaches of the Yellow River Basin area.

Performance Analysis. To utilize this acceleration structure, the execution time of program was reduced to a certain extent. For different mesh scale, the results are shown in Table 1 as follow.

Table 1 Execution time for each mesh scale

Mesh scale	CPU execution time[s]	GPU execution time[s]	Speed-up ratio
1025×1025	0.0309	0.0085	3.617
2049×2049	0.0747	0.0169	4.4193
4097×4097	0.3766	0.078	4.8282
8193×8193	1.4684	0.2979	4.9286

Speedup is the ratio between the runtime consumed by the same task while running respectively in the serial and parallel environments, which usually used to measure the evaluation of the efficiency of the procedure parallelizing. And the improved algorithm is based on the original algorithm, applying the SIMD parallel programming model to improve the efficiency of the algorithm. Here, the serial processing time refers to processing time consumed according to serial algorithm. From the perspective of algorithm analysis, the serial processing time of the algorithm can be decomposed into $TS=t_1+t_2$, in which t_1 is the runtime of the part of the serial program which was not executed parallel, while t_2 is the runtime of the other part in parallel mode. Parallel processing time calculated in this paper refers the total time of two parts—one is processing time of the part in the serial program that cannot be parallelized, and the other refers to the accelerated runtime of parallel processing data by using GPU. As a result, the formula used in this article to calculate the speedup ratio S is (1). The speed-up of these two algorithms is shown in Fig. 2.

$$S = \frac{T_s}{T_p} = \frac{t_1 + t_2}{t_1 + t_{dp}} \quad \begin{array}{l} T_s : \text{Execution time for original algorithm} \\ T_p : \text{Execution time for improved algorithm} \end{array} \quad (1)$$

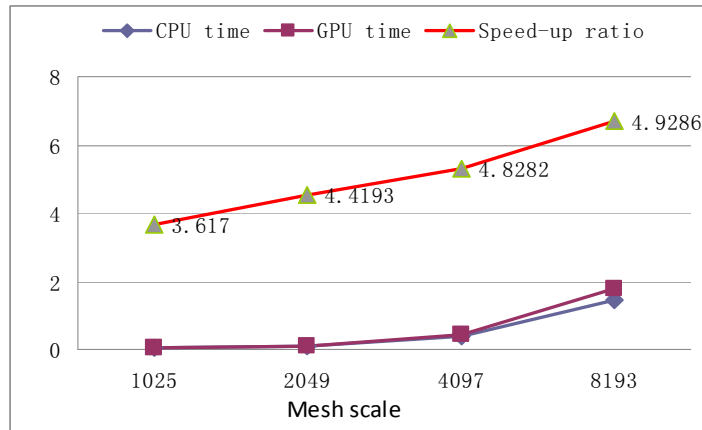


Fig. 2 Execution efficiency and speed-up ratio of CPU and GPU for different mesh scale

Performance Evaluation for Improved Algorithm. For each scale of mesh, the speedup ratio we gained differs not quite, approximately between four and five times. We are fairly satisfied for those results as a matter of fact. Not only the efficiency of our algorithm has been enhanced to some extent, but also the improved algorithm can obtain satisfactory simulation results.

It is obviously that the speed-up of the improved algorithm does not have an unusual performance by tenfold or hundredfold. There are two main reasons to explicate: On the one hand, compared to utilize looping statements on CPU, this algorithm merely utilize index to obtain elevation values on GPU. The algorithm efficiency would not be improved not fairly obviously. On the other hand, different mesh scales mainly have each works in the same order of magnitude. The span of elevation for each terrain had the same granularity in 2,000 parts.

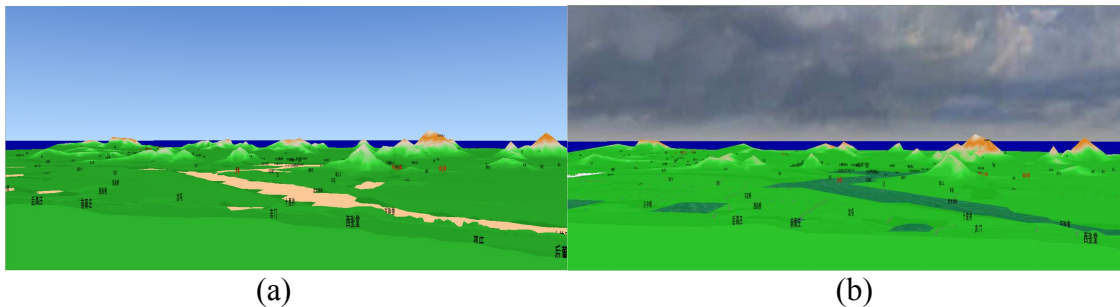


Fig. 3. Running Effect Picture of the same terrain: (a) CPU; (b) GPU

Running Effect Picture. The picture (b) generated by this improved algorithm is shown in Fig. 3 as follow. In contrast, picture (a) generated by the original algorithm. For these two pictures, I have to make an explanation. We added some extra display effects in generation of picture b. Both of them describe the same block in the Yellow River region nearby Puyang City in Henan Province.

Summary and Future Work

Based on these developments we have carried out a detailed solution to render terrain with elevation color. Experiments have proved that it is efficient to execute in terms of data parallel on GPU instead of CPU for this kind of algorithms. There are many reasons leading to low efficiency of terrain rendering visualization in VTP. We will keep on researching to modify more crucial algorithms for better performance.

Acknowledgment

The research was supported in part by the project Early Warning System of Water Pollution for River Basin under Science & Technology Foundation of Xi'an (CXY1010), and Overall Design and Demonstration Research on Environmental Economic Policy in China under Ministry of Environmental Protection of the PRC (201109076).

References

- [1] Blow J. Terrain rendering at high levels of detail, Game Developer's Conference (2000).
- [2] Information on <http://vterrain.org>
- [3] Mark Deloura in: Game Programming Gems, Charles River Media, August 2000, p.451–p.453.
- [4] Andre LaMothe in: Focus on 3D Terrain Programming, edited by Premier Press (2002), p.16-p.55.
- [5] Losasso F, Hoppe H, Geometry clipmaps: Terrain rendering using nested regular grids, ACM Transactions on Graphics (2004).
- [6] Li.Z, Zhu.Q and Gold.C, Digital terrain modeling: principles and methodology (CRC Press. Boca Raton 2009).
- [7] Christian Dick, Jens Krüger, and Rüdiger Westermann, GPU Ray-Casting for Scalable Terrain Rendering. EUROGRAPHICS 2009 (2009).
- [8] Xie Maojin, Wei Quncao, A Hardware Accelerated Algorithm for Terrain Visualization, Universal Access in Human-Computer Interaction. Lecture Notes in Computer Science, Vol. 5616 (2009), p.271-p.280.
- [9] Yacine Amara, Xavier Marsault, A GPU Tile-Load-Map architecture for terrain rendering: theory and applications, The Visual Computer Vol.25 (2009), p.805-p.824.
- [10] Schneider J, Westermann R. GPU-friendly high-quality terrain rendering, Journal of WSCG (2006).
- [11] Kalyan S. Perumalla, Brandon G. Aaby, Data Parallel Execution Challenges and Runtime Performance of Agent Simulations on GPUs, Proceedings of the Spring Simulation Multi-Conference (2008).

Experimental evaluation on the effect of the position of the nozzle in end milling under minimum quantity lubrication condition

Songmei Yuan^{1, a}, Si Liu^{1, b}, Lutao Yan^{1, c} and Qingchun Xiong^{2, d}

¹School of Mechanical Engineering and Automation, Beihang University, Beijing, 100191, China

²Chengdu Aircraft Industrial Group Co., Ltd.

^ayuansm@buaa.edu.cn, ^bliusiperfect@126.com, ^cltyan_buaa@163.com, ^dXiongqingchun@163.com

Keywords: Minimum Quantity Lubrication (MQL), nozzle position, end milling

Abstract. Stricter environmental regulations are making the use of an ample amount of conventional coolant impossible because of its negative impact on the environment. Consequently, the use of minimum quantity lubrication (MQL) has been regarded as a promising alternative to conventional fluid coolant applications. Despite several studies, there have been a few investigations about the influence of the MQL nozzle position, such as distance from tool-workpiece contact zone, elevation angles, the included angle between jet direction and feed direction. The current study presents experimental investigations on influences of the above parameters on performance in end milling. Tool wear and surface roughness are experimentally studied to compare the effects of different positions. The results show that the setting location of the nozzle is an important factor regarding the effective application of MQL oil mist.

Introduction

Copious amount of fluid flushed into the cutting zone at a low pressure from the back side of the chip is the most common way of applying coolants for attaining better tool life, surface finish and lower cutting force. Despite many advantages of the cutting fluid in machining processes, there is a serious concern about ecological and economical problems. Using cutting fluid is not only the main source of environmental pollution but it also brings about manufacturing cost increase, which is involved with cutting fluids (purchasing, recycling, chip drying, etc.) [1]. Hence, multitude researches have been guided in the last few decades to reduce or even eliminate the use of cutting fluids [2~6]. But there is still a long way to go before the cutting fluid can be considered totally harmless and acceptable [7]. In order to minimize the consequences of their use, the most reasonable step should be to reduce the consumption of the cutting fluids. So, minimum quantity lubricant has been considered as an appropriate alternative to conventional machining with flood cutting fluid supply [8].

Structure alloy steel has been widely applied to various mechanical parts and engineering components for its appropriate hardenability and higher strength. This paper chooses 50CrMnMo structure alloy steel as the experimental material. Minimum quantity lubrication (MQL) cutting technology shows huge advantage in various machining ways (turning, milling, grinding, drilling, etc.). The major objective of the present work is to study the effect of MQL nozzle position (including distance from tool-workpiece contact zone and elevation angles) on tool wear and surface roughness during milling of 50CrMnMo alloy. In addition, the influence of the included angle between jet direction and feed direction has been considered.

Experimental set up and conditions

Machining tests were performed on 50CrMnMo structure alloy steel with the chemical composition of Cr (1.40~1.80)%, Mo (0.20~0.60)%, C (0.45~0.55)%, Si (0.20~0.60)%, Mn (1.30~1.70)%, P≤0.030%, S≤0.030%, Bal.

The MQL system in this work has been designed, fabricated and used. Oil was atomized at the nozzle tip area and impinged to the cutting zone with high velocity. The experimental conditions are given in Table 1.

Table 1 Experimental conditions

Machine tool	XK7132 CNC milling machine, China
Work piece	50CrMnMo structure alloy steel
Cutting tool	EM20-160-C20-2T, Zhuzhou, China Diameter 20mm Two teeth
Inserts	coated cemented carbide
Cutting velocity	220[m/min]
Depth of cut	0.5[mm]
Width of cut	8[mm]
Feed rate	0.14[mm/rev]
MQL supply	Oil: 20[ml/h] , Air: 280[L/min], 0.35[MPa]
Elevation angles of MQL nozzle	30°, 45°, 60°
Distance between nozzle and cutting zone	10[mm], 20[mm], 30[mm]
Included angle between jet direction and feed direction	0°, 60°, 120°, 180°
Wet conditions	7 spindle oil
Environment	Wet; Dry; MQL

The schematic view of the experimental set up is shown in Fig. 1. High compressed drier air is provided by an external compressor and fed into the MQL device. MQL oil stream impinge through the nozzles at the cutting zone.

Tool wear progression at a predetermined location was measured after each subsequent pass using a toolmaker's microscope and a CCD camera. The surface roughness during each cut was measured with a surface roughness tester (TR101) under different cutting conditions.